Research Internship

Formal stability analysis of a PID-based control system for bidirectional heat transfer stations

In partial fulfillment of the requirements for the degree Master of Science
at the TUM School of Computation, Information and Technology
of the Technical University of Munich.

Institute	Munich Institute of Integrated Materials, Energy and Process Engineering (MEP)
	Lichtenbergstraße 4
	85748 Garching
Advisor	Prof. Dr. rer. nat. Thomas Hamacher
	M.Sc. Thomas Licklederer
Submitted by	Sarah Schmidt
Submitted on	Garching, March 3rd, 2023

Abstract

Smart Thermal Grids are a novel way to design our heating system and are based on bi-directional water flows between prosumers. The dual role of prosumers and the bi-directional heat transfer make controlling the system crucial to meet temperature and heat flow requirements. For this purpose, a weighted PID field control approach has already been devised and tested. The aim of this work resides in providing a formal stability analysis of the control system.

For this, we first establish a model of the simplest Smart Thermal Grid case of two prosumers and implement the field control approach. Regarding the stability analysis, different methods shall be investigated especially Lyapunov's direct and indirect method and Nyquist's stability criterion. To account for the lack of accuracy of the linearization of the Smart Thermal Grid over all possible inputs, a statistics based Monte-Carlo approach is further studied in combination with previously mentioned methods. Moreover, the idea of replacing the closed-loop control system by an equivalent open-loop one – referred to as extended state-space – to apply open-loop stability methods in combination with the Monte-Carlo approach is also introduced.

The different approaches have not proven to be successful in the scope of this work and would need to be further investigated in future work. Thus, some empirical considerations shall be made to account for experimental findings on the stability.

keywords - **Smart Thermal Grids, bi-directional heat transfer, temperature and heat flow control, stability analysis, Monte-Carlo approach**

TOPIC FOR A STUDENT THESIS / PROJECT

Formal stability analysis of a PID-based control system for bidirectional heat transfer stations

Motivation and Background

Bidirectional heat transfer stations are an essential element to enable prosumer behavior in thermal networks as a part of smart energy systems. Previous research focuses on the operation of these transfer stations in networks where the thermo-hydraulic system state is dominated by central plants and thus transfer stations hardly influence each other. However, this is significantly different in thermal networks with a focus on the flexible energy exchange between peer prosumers. In former studies we proposed suitable network and substations designs and have shown that distributed actuators in the substations mutually influence each other. Further, it was

Figure 1: Illustration of the controlled system under investigation

shown that the overall thermohydraulic state is quite sensitive to the control of the distributed actuators and characterized by changing flow directions and velocities. This imposes new challenges for the network control and leads to the need of new control strategies for bidirectional transfer stations that meet the requirements of flexible prosumer energy exchange.
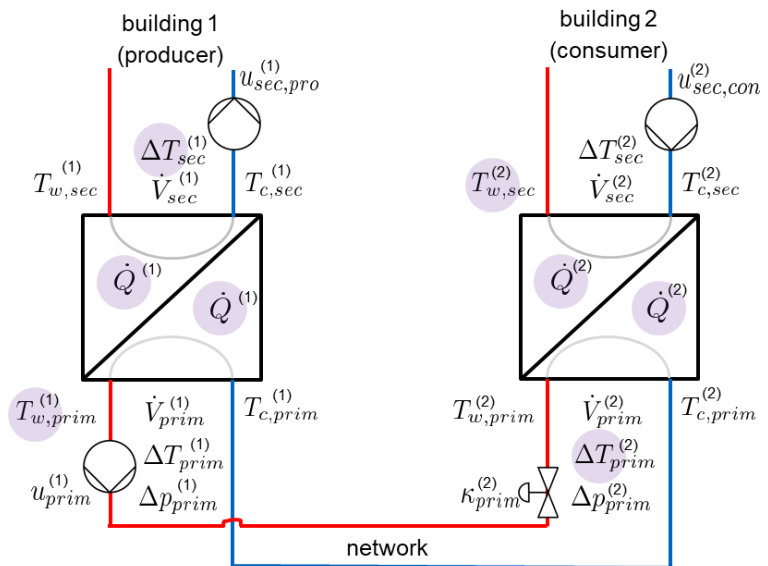
We propose a field-level control approach for pumps and valves of bidirectional heat transfer stations in prosumer-based heat networks. The control approach is based on PID controllers for the primary and secondary side of each substation. Weighted error-functions consider heat transfer setpoints and temperature objectives at the same time, thus relaxing the control problem.

Objectives and Tasks

The objective of this work is to perform a formal analytical stability analysis for a nonlinear control system that comprises bidirectional heat transfer stations (see example above) and proposed PID-controllers with weighted error functions.

1. Familiarization with the theory of formal stability analysis and the control system.
2. Mathematical representation of the controlled system by a system of equations and derivation of a suitable transfer function for the controlled system.
3. Mathematical representation of the whole control system by transfer functions.
4. Formal analytical stability analysis of the control system.
5. Conclusions on the conditions for system stability (& operability), on improvements of the control approach and on the behavior of more complex prosumer configurations

Requirements

- Profound knowledge in control theory and mathematical affinity
- Technical background in energy systems and thermal engineering

Contact for application: Thomas Licklederer (thomas.licklederer@tum.de)

Statement of academic integrity

I,

Last name: Schmidt
First name: Sarah
ID No.:   03695530

hereby confirm that the attached thesis,

Formal stability analysis of a PID-based control system for bidirectional heat transfer stations

was written independently by me without the use of any sources or aids beyond those cited, and all passages and ideas taken from other sources are indicated in the text and given the corresponding citation.
I confirm to respect the "Code of Conduct for Safeguarding Good Academic Practice and Procedures in Cases of Academic Misconduct at Technische Universität München, 2015", as can be read on the website of the Equal Opportunity Office of TUM.
Tools provided by the chair and its staff, such as models or programs, are also listed. These tools are property of the institute or of the individual staff member. I will not use them for any work beyond the attached thesis or make them available to third parties.

I agree to the further use of my work and its results (including programs produced and methods used) for research and instructional purposes.

I have not previously submitted this thesis for academic credit.

Garching, March 3rd, 2023

Declaration for the transfer of the thesis

I agree to the transfer of this thesis to:

- Students currently or in future writing their thesis at the chair:
  - ☐ Flat rate by employees
  - ☐ Only after particular prior consultation.
- Present or future employees at the chair
  - ☐ Flat rate by employees
  - ☐ Only after particular prior consultation.

My copyright and personal right of use remain unaffected.

Garching, March 3rd, 2023

Contents

Introduction

With the rapid expansion of renewable energies in the past decades, we face the challenge of integrating those fluctuating energy sources with low energy densities and high space requirements into the distribution grid. The local operation of PV panel and wind turbines, among the most widespread renewable energy generators, has brought up the idea of a decentral integration mechanism driven by sector coupling and an avoidance of long distance energy transport. Smart Grids then serve as a way of implementing these decentralized energy systems, by enabling local control and coordination between generation, transport and consumption. More precisely, Smart Grids are an infrastructure consisting of a grid for energy transport, sensor technology for recording the grid status in real-time and information and communication technologies for controlling the grid.

A fundamental aspect of those Smart Grids is the bi-directional energy flow between producers and consumers, which are able to change their role according to the current needs, in order to obtain a more optimal operation of the grid. The CoSES laboratory at the TU Munich [1] analyzes and simulates this concept on a small urban neighborhood scale of five buildings. Additionally to the integration of electricity and electric mobility, heating and cooling are also part the grid, which is the aspect we will be inspecting further in this report.

Indeed, Smart Thermal Grids aim at transforming our way of heating ourselves thanks to the bi-directional flow of water between neighborhood buildings. As a specific type of Smart Grid, it thus does also need to be controlled so as to ensure reliable water flows and accurate heating. A control approach for this has already be developed and tested by the CoSES laboratory, however, guaranteeing its stability is a crucial step to ensuring the reliability of the whole system. This thesis thus aims at conducting a formal stability analysis on the devised control approach with the objective to find out under which conditions the Smart Thermal Grid control system is stable.

The report has been written in the context of a Research Internship at the Munich Institute for Integrated Materials, Energy and Process Engineering. It reflects the work of 9 weeks worth of full-time research on the subject and complies with the internship conditions of the M.Sc. Electrical Engineering and Computer Science.

Chapter 1

The bi-directional heat transfer system

We look at the heat supply of residential buildings in an urban area. In the classical sense, such buildings are furnished with warm water by an external heater. The warm water inflow is not regulated with respect to the specific needs of the building, which might vary according to the time of day or season but also the individual actions of its inhabitants. An alternative heat transfer system, which favors a more optimal warm water flow by complying with specific building needs, has been introduced in the context of Smart Thermal Grids. In the following, we will be studying and deriving a model for this novel heat transfer system.

1.1   Concept and simplest case

The key idea behind Smart Thermal Grids is that a building can either be:

- a producer – the building does not need all the heat it has produced at a specific moment: it has a heat excess;

- or a consumer – the building has a lack of heat and cannot ensure the necessary heat supply for its inhabitants at a specific moment: it has a heat deficit.

We call a building capable of operating in both modes a prosumer. In our novel concept, all prosumers of a residential area – e.g. a neighborhood – are linked by a network of pipes, which allow a bi-directional water flow. This results in a heat exchange between prosumers according to their current mode – producer or consumer. Of course prosumers may also be idle, meaning that they neither need nor give heat and no water flow is associated with them, but we will not be considering this case in the framework of this report.

Indeed, in this report, we will be concentrating on what is to be considered the "simplest case" with only two buildings, as depicted in Figure 1.1. Building 1 functions as a producer and building 2 as a consumer. They are connected by one cold water and one warm water pipe. As said before, the water flow can be bi-directional in each pipe, however, as we fixed the role of the buildings in our setup, its direction is known to us: the warm water flows from building 1 to 2 and the cold water in the opposite direction. Each building has its own heating system, likewise comprised of one cold and one warm water pipe – further details are not of interest to us – and which communicates with the network via a plate heat exchanger. Heat is then transmitted from one side of the heat exchanger to the other without the pipes on either side being connected.

Looking back at the operating modes of our buildings, it can be seen that for building 1 heat is transferred from the warm water pipe of the secondary (building) side to the cold water pipe of the primary (network) side. This process heats up the cold water of the network, which is then conveyed to building 2 as warm water. Arriving at building 2, the heat is transmitted from the warm water pipe of the primary side to the cold water pipe of the secondary side. The water in the primary side being cold again it flows back to building 1, where the process is repeated. Building 2 now has warm water available.

Temperatures and thus heat exchange – as will be shown later on in the system model – can be regulated by the volume flow of the water. Pump and valves on each building and on each side let us control the volume flow in the network. On the network side, the producer is equipped with a pump and the consumer with a valve both located on the warm water pipe. On the secondary side, each prosumer has a pump on
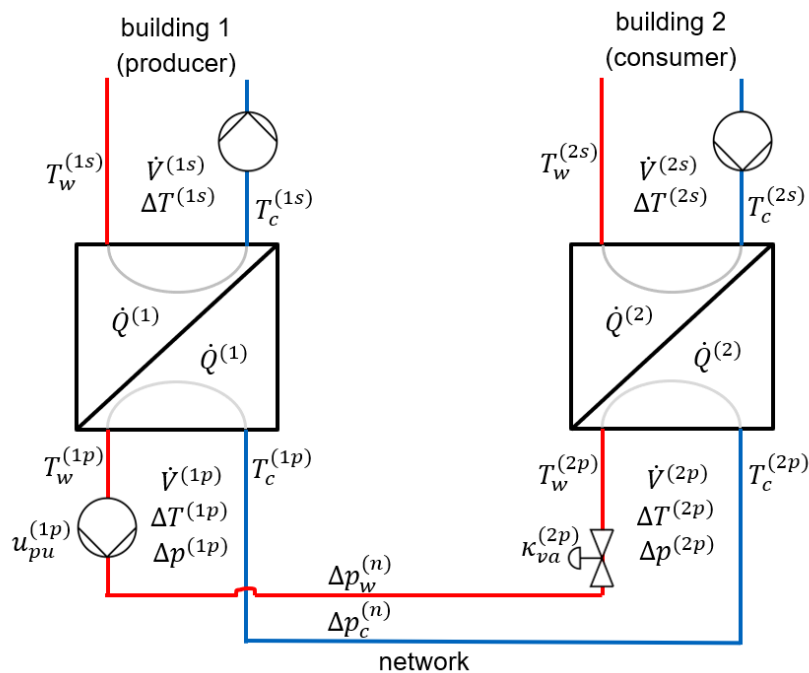
Figure 1.1: Simplest case scenario of a prosumer network

the cold water pipe, however, those are of little interest to as we do not look at the heating system of the building.

1.2   Deriving a model

The main feature of the system is that it is thermohydraulic. A model will accordingly be derived for both the hydraulic and the thermal system separately. The heat exchanger serves as link between both systems. The model that is derived in the following comes directly from [2], where the steady-state equations describing the system are set up. Notations used for deriving the model are summarized in Table 1.1, while configuration specific parameters are given in Table 1.2.

It shall also be noted that vectors will be indicated by lower case and matrices by upper case underlined symbols.

Physical variables	
a	hydraulic parameter
c_p	specific heat capacity of the fluid
κ	control variable for valve opening
Δp	pressure difference
$\dot{Q}$	heat flow
ρ	fluid density
$T, \Delta T$	temperature, temperature difference
τ	time delay
v	control variable for pump speed
$\dot{V}$	volume flow

Superscripts	
1	building 1
2	building 2
n	network
p	primary side
s	secondary side

Subscripts	
c	cold
hx	heat exchanger
hyd	hydraulic
is	current value
lin	linearized system
max	maximal value
$nlin$	nonlinear system
nom	nominal value
pi	pipe
pu	pump
$rand$	random
set	setpoint, desired or given value
ss	steady-state
tot	total
va	valve
w	warm

Table 1.1: Notations used for modeling the system

1.2.1 Hydraulic subsystem

In a first step, we look at the hydraulic part of the heat transfer system. Applying Kirchhoff's mesh rule for electrical circuits to the heat network, we get that the sum over all pressure differences in the system must be zero

$$\sum_i \Delta p_i = 0 \tag{1.1}$$

Looking at our heat transfer system in Figure 1.1, we thus get that

$$\underbrace{\Delta p^{(1p)}}_{\Delta p_{pu}^{(1p)} + \Delta p_{hx}^{(1p)} + \Delta p_{pi_w}^{(1p)} + \Delta p_{pi_c}^{(1p)}} + \underbrace{\Delta p^{(2p)}}_{\Delta p_{va}^{(2p)} + \Delta p_{hx}^{(2p)} + \Delta p_{pi_w}^{(2p)} + \Delta p_{pi_c}^{(2p)}} + \underbrace{\Delta p_w^{(n)}}_{\Delta p_{pi_w}^{(n)}} + \underbrace{\Delta p_c^{(n)}}_{\Delta p_{pi_c}^{(n)}} = 0 \tag{1.2}$$

Each pressure difference located in the network can further be decomposed into the pressure differences relative to each component present in the considered pipe portion, as done in (1.2). Ergo, we need to express the pressure difference associated with each hydraulic component – pump, valve, pipe and heat exchanger. In general, pressure differences can be directly linked to the volume flow by a function $\Delta p = f\left(\dot{V}\right)$, hence, we will be expressing f for each component. We further consider the following assumption on the volume flow.

Assumption 1 (Delay) *We only consider a delay in the volume flow through pumps and valves, while we assume pipes and heats exchanger to have an immediate volume flow. We also take that this delay in due to the volume flow in itself and not due to the actuation of pumps and valves.*

Pump We make use of pumps with variable speed drives, which can be controlled by the unified control variable v_{pu} – the normalized fluid speed. The pressure difference can be expressed with respect to the volume flow as follows

$$\Delta p_{pu} = a_{1_{pu}} \left(\dot{V}_{pu}\right)^2 + a_{2_{pu}} \left(v_{pu}\right)^2 - \tau_{pu} \frac{d\dot{V}_{pu}}{dt} \tag{1.3}$$

where

$$a_{1_{pu}} = \frac{\Delta p_{pu_{ref,1}} - \left(\frac{v_{pu_{ref,1}}}{v_{pu_{ref,2}}}\right)^2 \Delta p_{pu_{ref,1}}}{\left(\dot{V}_{pu_{ref,1}}\right)^2 - \left(\frac{v_{pu_{ref,1}}}{v_{pu_{ref,2}}}\right)^2 \left(\dot{V}_{pu_{ref,2}}\right)^2} \quad \text{and} \quad a_{2_{pu}} = \left(\frac{1}{v_{pu_{ref,1}}}\right)^2 \left[\Delta p_{pu_{ref,2}} - \left(\dot{V}_{pu_{ref,2}}\right)^2 a_{1_{pu}}\right]$$

are hydraulic parameters. It shall further be noted that unlike [2] and in accordance with Assumption 1, we added a delay in (1.3) to account for dynamics in the system as done in [3]. It has been modeled according to the characteristic curve of a pump – as the volume flow increases the pressure difference decreases – and can be tuned via τ_{pu}.

Valve We further use control valves for which we can address the drive by controlling the stroke. More precisely, we consider the control variable κ_{va}, which we take as the normalized flow factor of the stroke. The influence of the stroke on the volume flow and pressure difference is the following

$$\Delta p_{va} = a_{va} \frac{1}{(\kappa_{va})^2} \left(\dot{V}_{va}\right)^2 - \tau_{va} \frac{d\dot{V}_{va}}{dt} \tag{1.4}$$

with the hydraulic parameter

$$a_{va} = -10^3 \text{hPa} \frac{\rho}{1000\text{kg/m}^3} \frac{1}{(K_{vs})^2}$$

Again, we added the delay expressed by τ_{va} complying with Assumption 1 and the characteristic curve of the valve – as the volume flow increases the pressure difference decreases.

Pipe   We model pipes according to the Darcy-Weisbach equation as explained in [2] and get

$$\Delta p_{pi} = a_{pi} \left(\dot{V}_{pi} \right)^2 \tag{1.5}$$

with

$$a_{pi} = -\frac{8\rho}{\pi^2 \left(d_{pi} \right)^4} \left[\frac{L_{pi}}{d_{pi}} f_D + \zeta_{inst} \right]$$

where the Darcy-Weisbach friction factor f_D depends on the nominal Reynolds number $\mathrm{Re}_{nom} = \frac{\rho v_{pi_{nom}} d_{pi}}{\mu}$. Based on the Reynolds number range and thus the type of flow, f_D is expressed as follows:

- laminar flow ($\mathrm{Re}_{nom} \leq 2000$) – $f_D = \frac{64}{\mathrm{Re}_{nom}}$

- turbulent flow ($\mathrm{Re}_{nom} \geq 4000$) – $f_D = \dfrac{0.25}{\left[\log\left(\frac{\varepsilon}{3.7 d_{pi}} + \frac{5.74}{\left(\mathrm{Re}_{nom} \right)^{0.9}} \right) \right]^2}$

- transition regime ($2000 < \mathrm{Re}_{nom} < 4000$) – f_D then is the linear interpolation result between laminar and turbulent flow.

Heat exchanger   Last but not least, we consider plate heat exchangers, for which the pressure difference is quadratically proportional to the volume flow

$$\Delta p_{hx} = a_{hx} \left(\dot{V}_{hx} \right)^2 \tag{1.6}$$

with the hydraulic parameter

$$a_{hx} = -\frac{\left| \Delta p_{hx_{nom}} \right|}{\left(\dot{V}_{hx_{nom}} \right)^2}$$

Looking back at the pressure mesh rule in (1.2), we can insert equations (1.3) - (1.6), which leads us to the following equation for the volume flow

$$
\begin{aligned}
& a_{1_{pu}}^{(1p)} \left(\dot{V}^{(1p)} \right)^2 + a_{2_{pu}}^{(1p)} \left(v_{pu}^{(1p)} \right)^2 - \tau_{pu}^{(1p)} \frac{d\dot{V}^{(1p)}}{dt} \quad + a_{hx}^{(1)} \left(\dot{V}^{(1p)} \right)^2 + a_{pi_w}^{(1p)} \left(\dot{V}^{(1p)} \right)^2 \quad + a_{pi_c}^{(1p)} \left(\dot{V}^{(1p)} \right)^2 \\
& + a_{va}^{(2p)} \frac{1}{\left(\kappa_{va}^{(2p)} \right)^2} \left(\dot{V}^{(2p)} \right)^2 - \tau_{va}^{(2p)} \frac{d\dot{V}^{(2p)}}{dt} \quad + a_{hx}^{(2)} \left(\dot{V}^{(2p)} \right)^2 + a_{pi_w}^{(2p)} \left(\dot{V}^{(2p)} \right)^2 \quad + a_{pi_c}^{(2p)} \left(\dot{V}^{(2p)} \right)^2 \\
& \hspace{8cm} + a_{pi_w}^{(n)} \left(\dot{V}^{(2p)} \right)^2 \quad + a_{pi_c}^{(n)} \left(\dot{V}^{(1p)} \right)^2 = 0
\end{aligned}
\tag{1.7}
$$

Since we are only considering the simplest case with two prosumers, the volume flow through building 1 must be equal to the one through building 2. Adapting Kirchhoff's junction rule to hydraulic systems, we thus get that

$$\dot{V}^{(1p)} - \dot{V}^{(2p)} = 0 \tag{1.8}$$

Now, let us define the volume flow through the entire network as $\dot{V}^{(n)} = \dot{V}^{(1p)} = \dot{V}^{(2p)}$, then (1.7) becomes

$$
\begin{aligned}
& \underbrace{-\left(\tau_{pu}^{(1p)} + \tau_{va}^{(2p)} \right)}_{\tau_{hyd}} \frac{d\dot{V}^{(n)}}{dt} + \underbrace{\left(a_{1_{pu}}^{(1p)} + a_{hx}^{(1)} + a_{pi_w}^{(1p)} + a_{pi_c}^{(1p)} + a_{hx}^{(2)} + a_{pi_w}^{(2p)} + a_{pi_c}^{(2p)} + a_{pi_w}^{(n)} + a_{pi_c}^{(n)} \right)}_{a_{hyd}} \left(\dot{V}^{(n)} \right)^2 \\
& \hspace{4cm} + a_{2_{pu}}^{(1p)} \left(v_{pu}^{(1p)} \right)^2 + a_{va}^{(2p)} \left(\dot{V}^{(n)} \right)^2 \frac{1}{\left(\kappa_{va}^{(2p)} \right)^2} = 0
\end{aligned}
\tag{1.9}
$$

This equation describes the dynamics of the volume flow in the hydraulic subsystem. Due to the simplifications, which can be done in our case scenario, this dynamic is sufficient for describing the hydraulic behavior of the heat-transfer system.
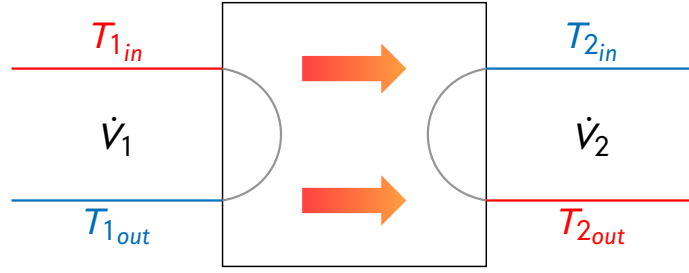
Figure 1.2: General heat exchanger scheme

1.2.2 Thermal subsystem

Now, let us have a look at the thermal subsystem. We make the following assumption for simplification purposes.

Assumption 2 (Losses) *We do not consider losses in the pipes, hence, we assume $\dot{Q}_{loss} = 0$ for heat flow losses.*

However, do note that losses do occur and this assumption lowers our precision in estimating temperatures. We can now assume that we only have a single warm and cold water temperature in the entire network, which we will denote $T_w^{(n)}$ and $T_c^{(n)}$ respectively and which can be expressed as

$$T_w^{(n)} = T_w^{(1p)} = T_w^{(2p)} \qquad \text{and} \qquad T_c^{(n)} = T_c^{(1p)} = T_c^{(2p)} \tag{1.10}$$

Moreover, we assume that there are no losses in the heat exchanger either, meaning that power is fully conveyed from building to network or vice-versa. As a result of this and Assumption 2, the heat flow that goes from building 1 into the network must be wholly conducted to building 2. Thus, we have a single heat flow through the entire system

$$\dot{Q}^{(n)} = \dot{Q}^{(1)} = \dot{Q}^{(2)} \tag{1.11}$$

Heat exchanger We model the counter current flow of the heat exchanger using the general nomenclature of Figure 1.2 as a reference – the subscript 1 refers to the source side and 2 to the sink side. It has to hold that

$$T_{1_{in}} > T_{1_{out}} > T_{2_{out}} > T_{2_{in}} \tag{1.12}$$

The resulting general dynamics stem from [2] while adding a delay as in [4]. We thus get for the heat exchanger in Figure 1.2

$$\tau_{hx}\frac{\mathrm{d}T_{1_{out}}}{\mathrm{d}t} + T_{1_{out}} = \left(1 - \chi_1\left(\dot{V}_1, \dot{V}_2\right)\right) T_{1_{in}} + \chi_1\left(\dot{V}_1, \dot{V}_2\right) T_{2_{in}} \tag{1.13}$$

$$\tau_{hx}\frac{\mathrm{d}T_{2_{out}}}{\mathrm{d}t} + T_{2_{out}} = \chi_2\left(\dot{V}_1, \dot{V}_2\right) T_{1_{in}} + \left(1 - \chi_2\left(\dot{V}_1, \dot{V}_2\right)\right) T_{2_{in}} \tag{1.14}$$

where $\chi_1\left(\dot{V}_1, \dot{V}_2\right)$ and $\chi_2\left(\dot{V}_1, \dot{V}_2\right)$ are functions of the volume flows on either side of the heat exchanger

$$\chi_1\left(\dot{V}_1, \dot{V}_2\right) = \frac{1 - \exp\left[\left(\frac{\dot{V}_1}{\dot{V}_2} - 1\right)\frac{k_{hx}A_{hx}}{\rho c_p \dot{V}_1}\right]}{1 - \frac{\dot{V}_1}{\dot{V}_2}\exp\left[\left(\frac{\dot{V}_1}{\dot{V}_2} - 1\right)\frac{k_{hx}A_{hx}}{\rho c_p \dot{V}_1}\right]} \qquad \text{and} \qquad \chi_2\left(\dot{V}_1, \dot{V}_2\right) = \frac{1 - \exp\left[\left(\frac{\dot{V}_2}{\dot{V}_1} - 1\right)\frac{k_{hx}A_{hx}}{\rho c_p \dot{V}_2}\right]}{1 - \frac{\dot{V}_2}{\dot{V}_1}\exp\left[\left(\frac{\dot{V}_2}{\dot{V}_1} - 1\right)\frac{k_{hx}A_{hx}}{\rho c_p \dot{V}_2}\right]}$$

Adapting this general scheme to our scenario, we get:

- Building 1 – source: secondary side $\quad \dot{V}_1 = \dot{V}^{(1s)}$; $\quad T_{1_{in}} = T_w^{(1s)}$; $\quad T_{1_{out}} = T_c^{(1s)}$
    sink: primary side $\quad \dot{V}_2 = \dot{V}^{(n)}$; $\quad T_{2_{in}} = T_c^{(n)}$; $\quad T_{2_{out}} = T_w^{(n)}$

Pump			
$v_{pu_{ref,1}}$	1	-	control var. ref. op. state 1
$\dot{V}_{pu_{ref,1}}$	0	L/min	volume flow ref. op. state 1
$\Delta p_{pu_{ref,1}}$	402.21	hPa	pressure diff. ref. op. state 1
$v_{pu_{ref,2}}$	1	-	control var. ref. op. state 2
$\dot{V}_{pu_{ref,2}}$	55.33	L/min	volume flow ref. op. state 2
$\Delta p_{pu_{ref,2}}$	0	hPa	pressure diff. ref. op. state 2
τ_{pu}	35	s	delay
Valve			
K_{vs}	2.5	m³/h	flow coeff. at full opening
τ_{va}	35	s	delay
Heat ex.			
$\Delta p_{hx_{nom}}$	155	hPa	loss at nom. mass flow rate
$\dot{V}_{hx_{nom}}$	21.504	L/min	nom. volume flow rate
A_{hx}	1.13	m²	heat transfer surface
k_{hx}	5270	W/(m² K)	nom. heat transfer coeff.
τ_{hx}	10	s	delay

Pipe 1			
L_{pi}	50	m	pipe length
d_{pi}	0.022	m	inner pipe diameter
ε	0.011	mm	roughness of inner pipe surface
ζ_{inst}	10	-	pressure loss coeff. for inst. in pipes
$u_{pi_{nom}}$	0.22	m/s	nom. flow velocity
Pipe 2			
L_{pi}	10	m	pipe length
d_{pi}	0.022	m	inner pipe diameter
ε	0.011	mm	roughness of inner pipe surface
ζ_{inst}	3.5	-	pressure loss coeff. for inst. in pipes
$v_{pi_{nom}}$	0.22	m/s	nom. flow velocity
Fluid			
ρ	1000	kg/m³	density of fluid
μ	1.0016	mPa s	dynamic viscosity
c_P	4200	J/(kg K)	specific isobaric heat capacity

Table 1.2: Setup parameters

- Building 2 – source: primary side $\quad \dot{V}_1 = \dot{V}^{(n)}\,; \quad T_{1_{in}} = T_w^{(n)}\,; \quad T_{1_{out}} = T_c^{(n)}$
  sink: secondary side $\quad \dot{V}_2 = \dot{V}^{(2s)}\,; \quad T_{2_{in}} = T_c^{(2s)}\,; \quad T_{2_{out}} = T_w^{(2s)}$

Hence, we get four dynamic equations describing the four – under Assumption 2 – temperatures in the system. In total we now have five dynamic equations describing the whole thermohydraulic heat transfer system and which will serve for setting up a state-space model in section 1.3.

1.2.3 Remarks on the setup

However, before that, let us make a few remarks on our specific configuration. Most details on specific values can be gathered from Table 1.2, yet some clarifications remain to be made.

Concerning the pipes, we differentiate two types of pipes in Table 1.2: pipe 1 refers to the pipes of the network i.e. the warm or cold water pipe, while pipe 2 refers to the pipe portion liking the network to the building. Here, pipe 2 includes both the warm and cold water pipe so the hydraulic parameter sums $a_{pi_w}^{(1p)} + a_{pi_c}^{(1p)}$ and $a_{pi_w}^{(2p)} + a_{pi_c}^{(2p)}$ in equation (1.9) are described by this single pipe.

It shall also be noted that all pumps, valve or heat exchangers in the setup are chosen to be identical and can thus be described by this single parameter set.

1.3 State-space representation

In order to design a controller and evaluate the stability of the system in later steps, we need to express the system behavior in a state-space representation of the form

$$\dot{\underline{x}} = \underline{f}\left(\underline{x}, \underline{u}\right) \tag{1.15}$$

$$\underline{y} = \underline{h}\left(\underline{x}, \underline{u}\right) \tag{1.16}$$

$\underline{f}$ and $\underline{h}$ are nonlinear function which need to be determined, while $\underline{x} \in \mathcal{X} \subseteq \mathbb{R}^{\dim(\underline{x})}$ are the states, $\underline{u} \in \mathcal{U} \subseteq \mathbb{R}^{\dim(\underline{u})}$ the inputs and $\underline{y} \in \mathcal{Y} \subseteq \mathbb{R}^{\dim(\underline{y})}$ the outputs of the system. We further highlight that in our framework we have a time-invariant system.

1.3.1 Nonlinear model

The nonlinear state-space model stems directly from the dynamics equations – (1.9), (1.13) and (1.14) – set up in the previous section.

States We define the five changing variables as our states, hence, we get the following state vector

$$\underline{x} = \begin{bmatrix} x_1 \\ x_2 \\ x_3 \\ x_4 \\ x_5 \end{bmatrix} = \begin{bmatrix} \dot{V}^{(n)} \\ T_w^{(n)} \\ T_c^{(n)} \\ T_c^{(1s)} \\ T_w^{(2s)} \end{bmatrix} \tag{1.17}$$

Inputs It is possible for us to control pump speeds and valve openings. Nonetheless, as we consider the building heating system to be a "black box" to us, we assume for the model that we control its volume flow as a whole and not the individual pumps. For the same reason, we cannot influence the inlet building temperatures with our heat transfer scenario; still we regard them as inputs due to their influence on our system. This leads us to the following input vector

$$\underline{u} = \begin{bmatrix} u_1 \\ u_2 \\ u_3 \\ u_4 \\ u_5 \\ u_6 \end{bmatrix} = \begin{bmatrix} v_{pu}^{(1p)} \\ \kappa_{va}^{(2p)} \\ \dot{V}^{(1s)} \\ \dot{V}^{(2s)} \\ T_w^{(1s)} \\ T_c^{(2s)} \end{bmatrix} \tag{1.18}$$

Outputs Finally, we express the output vector[1] as

$$\underline{y} = \begin{bmatrix} y_1 \\ y_2 \\ y_3 \\ y_4 \\ y_5 \end{bmatrix} = \begin{bmatrix} \dot{Q}^{(n)} = \rho c_p \dot{V}^{(n)} \Delta T^{(n)} \\ T_w^{(2s)} \\ \Delta T^{(n)} = T_w^{(n)} - T_c^{(n)} \\ \Delta T^{(1s)} = T_w^{(1s)} - T_c^{(1s)} \\ T_w^{(n)} \end{bmatrix} \tag{1.19}$$

From this we directly get our nonlinear state-space representation in the form given in (1.15)

$$\underline{\dot{x}} = \begin{bmatrix} \dot{x}_1 \\ \dot{x}_2 \\ \dot{x}_3 \\ \dot{x}_4 \\ \dot{x}_5 \end{bmatrix} = \begin{bmatrix} f_1\left(\underline{x},\underline{u}\right) \\ f_2\left(\underline{x},\underline{u}\right) \\ f_3\left(\underline{x},\underline{u}\right) \\ f_4\left(\underline{x},\underline{u}\right) \\ f_5\left(\underline{x},\underline{u}\right) \end{bmatrix} = \begin{bmatrix} -\frac{a_{hyd}}{\tau_{hyd}} x_1^2 - \frac{a_{2pu}^{(1p)}}{\tau_{hyd}} u_1^2 - \frac{a_{va}^{(2p)}}{\tau_{hyd}} \frac{x_1^2}{u_2^2} \\ \frac{1}{\tau_{hx}}\left(\chi_2^{(1)}(x_1,u_3)\,u_5 + \left(1 - \chi_2^{(1)}(x_1,u_3)\right)x_3 - x_2\right) \\ \frac{1}{\tau_{hx}}\left(\left(1 - \chi_1^{(2)}(x_1,u_4)\right)x_2 + \chi_1^{(2)}(x_1,u_4)\,u_6 - x_3\right) \\ \frac{1}{\tau_{hx}}\left(\left(1 - \chi_1^{(1)}(x_1,u_3)\right)u_5 + \chi_1^{(1)}(x_1,u_3)\,x_3 - x_4\right) \\ \frac{1}{\tau_{hx}}\left(\chi_2^{(2)}(x_1,u_4)\,x_2 + \left(1 - \chi_2^{(2)}(x_1,u_4)\right)u_6 - x_5\right) \end{bmatrix} \tag{1.20}$$

with

$$\chi_1^{(1)}(x_1,u_3) = \frac{1 - \exp\left[\left(\frac{u_3}{x_1} - 1\right)\frac{k_{hx}A_{hx}}{\rho c_p u_3}\right]}{1 - \frac{u_3}{x_1}\exp\left[\left(\frac{u_3}{x_1} - 1\right)\frac{k_{hx}A_{hx}}{\rho c_p u_3}\right]} \quad ; \quad \chi_2^{(1)}(x_1,u_3) = \frac{1 - \exp\left[\left(\frac{x_1}{u_3} - 1\right)\frac{k_{hx}A_{hx}}{\rho c_p x_1}\right]}{1 - \frac{x_1}{u_3}\exp\left[\left(\frac{x_1}{u_3} - 1\right)\frac{k_{hx}A_{hx}}{\rho c_p x_1}\right]}$$

$$\chi_1^{(2)}(x_1,u_4) = \frac{1 - \exp\left[\left(\frac{u_4}{x_1} - 1\right)\frac{k_{hx}A_{hx}}{\rho c_p u_4}\right]}{1 - \frac{u_4}{x_1}\exp\left[\left(\frac{u_4}{x_1} - 1\right)\frac{k_{hx}A_{hx}}{\rho c_p u_4}\right]} \quad ; \quad \chi_2^{(2)}(x_1,u_4) = \frac{1 - \exp\left[\left(\frac{x_1}{u_4} - 1\right)\frac{k_{hx}A_{hx}}{\rho c_p x_1}\right]}{1 - \frac{x_1}{u_4}\exp\left[\left(\frac{x_1}{u_4} - 1\right)\frac{k_{hx}A_{hx}}{\rho c_p x_1}\right]}$$

---

[1]Explanations concerning the choice of the output variables will later be given in chapter 2.

The output vector (1.19) is already formulated as required from (1.16)

$$\underline{y} = \begin{bmatrix} y_1 \\ y_2 \\ y_3 \\ y_4 \\ y_5 \end{bmatrix} = \begin{bmatrix} h_1\left(\underline{x}, \underline{u}\right) \\ h_2\left(\underline{x}, \underline{u}\right) \\ h_3\left(\underline{x}, \underline{u}\right) \\ h_4\left(\underline{x}, \underline{u}\right) \\ h_5\left(\underline{x}, \underline{u}\right) \end{bmatrix} = \begin{bmatrix} \rho c_p x_1 \left(x_2 - x_3\right) \\ x_5 \\ x_2 - x_3 \\ u_5 - x_4 \\ x_2 \end{bmatrix} \tag{1.21}$$

1.3.2 Linearizing the system

While the previously derived nonlinear system dynamics are a fairly accurate representation of the Smart Thermal Grid behavior, they are not easily manipulable in the context of stability analysis. For this reason, we aim at expressing our nonlinear state-space equations (1.20) and (1.21) as an LTI[2] system.

For this, we redefine our states as having a large signal and a small signal component, so that $\underline{x} = \underline{x}^* + \Delta\underline{x}$. The large signal term $\underline{x}^*$ is to be the understood as the operating point around which we linearize. The same partition holds for the inputs and outputs, thus we get $\underline{u} = \underline{u}^* + \Delta\underline{u}$ and $\underline{y} = \underline{y}^* + \Delta\underline{y}$. By approximation of (1.15) and (1.16) by a Taylor series around the operating point, we get the following expression for the linearized (small signal) model (see [5] for more details on the procedure)

$$\Delta\underline{\dot{x}} = \underline{A}\,\Delta\underline{x} + \underline{B}\,\Delta\underline{u} \qquad \Rightarrow \qquad \underline{\dot{x}} = \underline{A}\left(\underline{x} - \underline{x}^*\right) + \underline{B}\left(\underline{u} - \underline{u}^*\right) \tag{1.22}$$

$$\Delta\underline{y} = \underline{C}\,\Delta\underline{x} + \underline{D}\,\Delta\underline{u} \qquad \Rightarrow \qquad \underline{y} = \underline{C}\left(\underline{x} - \underline{x}^*\right) + \underline{D}\left(\underline{u} - \underline{u}^*\right) + \underline{y}^* \tag{1.23}$$

under the assumption that $\underline{\dot{x}}^* = 0$. We further introduce $\underline{A} \in \mathbb{R}^{\dim(\underline{x}) \times \dim(\underline{x})}$ as the system matrix, $\underline{B} \in \mathbb{R}^{\dim(\underline{x}) \times \dim(\underline{u})}$ as the input matrix, $\underline{C} \in \mathbb{R}^{\dim(\underline{y}) \times \dim(\underline{x})}$ as the output matrix and $\underline{D} \in \mathbb{R}^{\dim(\underline{y}) \times \dim(\underline{u})}$ as the feedthrough matrix. Those matrices are different Jacobians of $\underline{f}$ and $\underline{h}$.

We establish the general expression of the Jacobian through the computation of the state matrix $\underline{A}$. It is defined as follows and evaluated at a chosen operating point denoted as before as $\underline{x}^*, \underline{u}^*$

$$\underline{A} = \left.\frac{\partial \underline{f}}{\partial \underline{x}}\right|_{\underline{x}^*, \underline{u}^*} = \left.\begin{bmatrix} \frac{\partial f_1}{\partial x_1} & \cdots & \frac{\partial f_1}{\partial x_i} & \cdots & \frac{\partial f_1}{\partial x_{\dim(\underline{x})}} \\ \vdots & \ddots & & & \vdots \\ \frac{\partial f_{\dim(\underline{x})}}{\partial x_1} & \cdots & \frac{\partial f_{\dim(\underline{x})}}{\partial x_i} & \cdots & \frac{\partial f_{\dim(\underline{x})}}{\partial x_{\dim(\underline{x})}} \end{bmatrix}\right|_{\underline{x}^*, \underline{u}^*} \tag{1.24}$$

Taking our nonlinear state-space equations (1.20) and applying the formula above, we get the following system matrix

$$\underline{A} = \left.\begin{bmatrix} -2\frac{a_{hyd}}{\tau_{hyd}}x_1 - 2\frac{a_{va}^{(2p)}}{\tau_{hyd}}\frac{x_1}{u_2^2} & 0 & 0 & 0 & 0 \\ \frac{\frac{\partial \chi_2^{(1)}(x_1, u_3)}{\partial x_1}(d_1 - x_3)}{\tau_{hx}} & -\frac{1}{\tau_{hx}} & \frac{1 - \chi_2^{(1)}(x_1, u_3)}{\tau_{hx}} & 0 & 0 \\ \frac{\frac{\partial \chi_1^{(2)}(x_1, u_4)}{\partial x_1}(-x_2 + d_2)}{\tau_{hx}} & \frac{1 - \chi_1^{(2)}(x_1, u_4)}{\tau_{hx}} & -\frac{1}{\tau_{hx}} & 0 & 0 \\ \frac{\frac{\partial \chi_1^{(1)}(x_1, u_3)}{\partial x_1}(-d_1 + x_3)}{\tau_{hx}} & 0 & \frac{\chi_1^{(1)}(x_1, u_3)}{\tau_{hx}} & -\frac{1}{\tau_{hx}} & 0 \\ \frac{\frac{\partial \chi_2^{(2)}(x_1, u_4)}{\partial x_1}(x_2 - d_2)}{\tau_{hx}} & \frac{\chi_2^{(2)}(x_1, u_4)}{\tau_{hx}} & 0 & 0 & -\frac{1}{\tau_{hx}} \end{bmatrix}\right|_{\underline{x}^*, \underline{u}^*} \tag{1.25}$$

The remaining matrices of the LTI system (1.22), (1.23) can be computed in a similar way. Indeed, the input matrix equals to the Jacobian of (1.20) with respect to the input

---

[2]Linear Time-Invariant.

$$\underline{B} = \left.\frac{\partial \underline{f}}{\partial \underline{u}}\right|_{\underline{x}^*,\,\underline{u}^*} = \left.\begin{Vmatrix} \frac{-2a_{2pu}^{(1p)}}{\tau_{hyd}}u_1 & \frac{-2a_{va}^{(2p)}}{\tau_{hyd}}\frac{x_1^2}{u_2^3} & 0 & 0 & 0 & 0 \\[2mm] 0 & 0 & \frac{\frac{\partial \chi_2^{(1)}(x_1,u_3)}{\partial u_3}(d_1-x_3)}{\tau_{hx}} & 0 & \frac{\chi_2^{(1)}(x_1,u_3)}{\tau_{hx}} & 0 \\[2mm] 0 & 0 & 0 & \frac{\frac{\partial \chi_1^{(2)}(x_1,u_4)}{\partial u_4}(-x_2+d_2)}{\tau_{hx}} & 0 & \frac{\chi_1^{(2)}(x_1,u_4)}{\tau_{hx}} \\[2mm] 0 & 0 & \frac{\frac{\partial \chi_1^{(1)}(x_1,u_3)}{\partial u_3}(-d_1+x_3)}{\tau_{hx}} & 0 & \frac{1-\chi_1^{(1)}(x_1,u_3)}{\tau_{hx}} & 0 \\[2mm] 0 & 0 & 0 & \frac{\frac{\partial \chi_2^{(2)}(x_1,u_4)}{\partial u_4}(x_2-d_2)}{\tau_{hx}} & 0 & \frac{1-\chi_2^{(2)}(x_1,u_4)}{\tau_{hx}} \end{Vmatrix}\right|_{\underline{x}^*,\,\underline{u}^*} \tag{1.26}$$

Meanwhile, the output and feedthrough matrices stem from the nonlinear function $\underline{h}$ in (1.21)

$$\underline{C} = \left.\frac{\partial \underline{h}}{\partial \underline{x}}\right|_{\underline{x}^*,\,\underline{u}^*} = \left.\begin{Vmatrix} \rho c_p(x_2 - x_3) & \rho c_p x_1 & -\rho c_p x_1 & 0 & 0 \\ 0 & 0 & 0 & 0 & 1 \\ 0 & 1 & -1 & 0 & 0 \\ 0 & 0 & 0 & -1 & 0 \\ 0 & 1 & 0 & 0 & 0 \end{Vmatrix}\right|_{\underline{x}^*,\,\underline{u}^*} \tag{1.27}$$

$$\underline{D} = \left.\frac{\partial \underline{h}}{\partial \underline{u}}\right|_{\underline{x}^*,\,\underline{u}^*} = \begin{bmatrix} 0 & 0 & 0 & 0 & 0 & 0 \\ 0 & 0 & 0 & 0 & 0 & 0 \\ 0 & 0 & 0 & 0 & 0 & 0 \\ 0 & 0 & 0 & 0 & 1 & 0 \\ 0 & 0 & 0 & 0 & 0 & 0 \end{bmatrix} \tag{1.28}$$

1.3.3 Evaluation of the linearized model

As a linearization is only a planar approximation of the system dynamics around an operating point, we should evaluate its quality. By quality we understand the difference between the nonlinear and linearized system behavior at points other than the operating point especially when reaching steady-state. Hence, we choose to examine the absolute error of the steady-state value of each state. Due to the different natures of the states, we need to define two types of errors:

- the volume flow steady-state error – $e_{ss,\dot{V}} = \dot{V}_{ss,nlin} - \dot{V}_{ss,lin}$;
- the temperature steady-state error – $e_{ss,T} = T_{ss,nlin} - T_{ss,lin}$.

We aim at comparing these errors for two different operating points, which are given in Table 1.3. Operating point 1 linearizes the system around high pump/valve openings, volume flows and temperature inputs whereas operating point 2 does this for low volume flows and temperatures. The operating point states come from the simulated steady-state values of the nonlinear system for the given inputs.

Errors for random inputs In order to compare the quality of the operating points, we look at both the linear and nonlinear system response for 500 uniformly distributed random draws of the input vector $\underline{u}$. Individual inputs are drawn in the following intervals

$$u_1 \in [0.1, 1] \,,\; u_2 \in [0.1, 1] \,,\; u_3 \in [2, 15]\,\text{L/min}\,,\; u_4 \in [2, 15]\,\text{L/min}\,,\; u_5 \in [40, 90]\,°\text{C}\,,\; u_6 \in [30, 70]\,°\text{C}$$

For each simulation, we then compute the errors as defined above. Figure 1.3 shows these errors for the 500 random draws for each state. The mean error for each state as well as its standard deviation are additionally indicated by the black errorbars and their values provided in Table 1.3.

Looking at the results in Figure 1.3, we can stem that the error for the volume flow $e_{ss,\dot{V}}$ is very low for both operating points – indeed the mean error is $|0.02\text{L/min}|$ and the standard deviation inferior to 0.1L/min in both cases. Furthermore, the highest error value is of -0.59L/min for operating point 1 and of -0.57L/min for

		u_1	u_2	u_3	u_4	u_5	u_6	x_1	x_2	x_3	x_4	x_5
OP 1	Value	0.8	0.9	12L/min	12L/min	75°C	65°C	8.56L/min	74.83°C	65.17°C	68.11°C	71.89°C
	Mean error							−0.02L/min	−1.71K	1.68K	2.11K	−2.22K
	Error stand. dev.							0.06L/min	4.62K	4.59K	5.64K	5.70K
OP 2	Value	0.4	0.5	5L/min	5L/min	60°C	45°C	4.27L/min	59.88°C	45.12°C	47.40°C	57.60°C
	Mean error							−0.02L/min	−1.75K	1.43K	3.03K	−2.98K
	Error stand. dev.							0.05L/min	5.10K	4.34K	8.68K	9.34K

Table 1.3: Comparison of two operating points (OP)

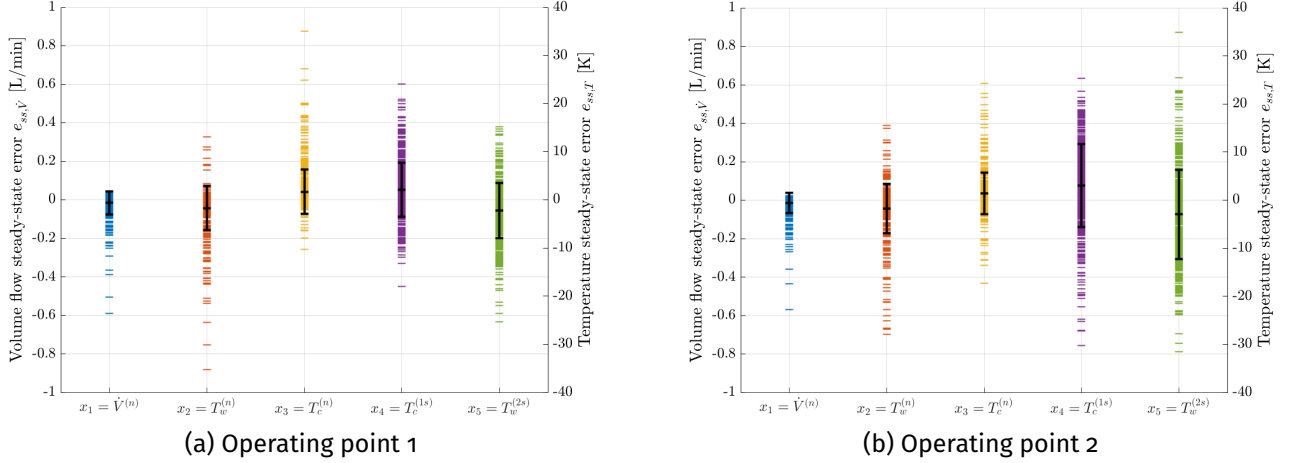(a) Operating point 1   (b) Operating point 2

Figure 1.3: Absolute steady-state errors $e_{ss,\dot{V}}$ and $e_{ss,T}$ obtained by randomly generating 500 input vectors $\underline{u}$ from a uniform distribution. The black errorbars represent the mean error and standard deviation.

operating point 2; we deem this to be still close to the nonlinear system dynamics and thus both operating points to be a good linear approximation for the volume flow.

Now looking at the error for the temperature $e_{ss,T}$, the mean error reaches up to $|2.22\text{K}|$ for operating point 1 and up to $|3.03\text{K}|$ for operating point 2. While this can still be considered to be close enough to the nonlinear steady-state value, the standard deviation for both operating points for the network temperatures – $T_w^{(n)}$ and $T_c^{(n)}$ – is of approximately $4-5\text{K}$. In addition for the building temperatures – $T_c^{(1s)}$ and $T_w^{(2s)}$ – it is of around 5.7K for the first operating point and 9K for the second one. In both cases, we hence reach high errors, even more so for operating point 2. This difference in the absolute building temperature errors between both operating points might be explained by the lower volume flow value around which we linearize for operating point 2.

Finally, we consider operating point 1 to be the better linearization choice according to our study, as statistically it has the lower temperature error.

Errors for individual inputs   In a second step, we aim at understanding the influence of individual inputs on the errors. For this, we set each input to their operating point value as given in Table 1.3 and vary a single input in the allowed interval given above. The resulting volume flow and temperature errors of this procedure are plotted for each input separately in Figure 1.4.

First of all, looking at the plots, we see that the error values obtained in Figure 1.4 tend to confirm our previous analysis. We can further make some general findings on both operating points. It is thus particularly striking that the inputs u_5 and u_6, which correspond to the secondary side input temperatures, generate no steady-state errors whatsoever on the considered interval. This can be explained by the fact that the nonlinear system is linear with respect to these two inputs when considering the other inputs to be constant. Moreover, the errors are smallest/ null around the operating point, as is to be expected as by linearizing we create a planar approximation of the nonlinear system around the operating point.

Overall, the errors are low for operating point 1 and high for operating point 2 for high pump/ valve openings and high secondary side volume flows and vice-versa. This is hardly surprising since operating point 1 linearizes the system around high input values and operating point 2 around low input values. Yet it can be observed that the error absolute values tend to be much higher for operating point 2 (with the

exception of the volume flow error for state x_1 which reaches up to $|0.5\text{L/min}|$ for operating point 1 for small valve openings u_2). Indeed, for high pump openings u_1, temperature errors can go up to $|17\text{K}|$ for operating point 2, which is due to the much higher network volume flow this generates in comparison with the operating point network volume flow. Similarly, as the relation between temperatures and volume flows is highly nonlinear, the temperature errors reach up to $|17\text{K}|$ for very high building input volume flows u_3 and u_4. It can also be noticed that this extreme error is achieved for the temperature state corresponding to the same building as the varied input – i.e. the error for state $x_4 = T_c^{(1s)}$ for a big volume flow $u_3 = \dot{V}^{(1s)}$ is approximately -17K.

Ultimately, this analysis confirms that the linearization around operating point 1 tends to be more accurate than the one around operating point 2 on the overall considered intervals. Yet, the high errors we can achieve for temperatures even for this "better" operating point, raises the question of the relevance of the linearization and thus the validity of our linearized state-space representation on the entire set of possible inputs $\mathcal{U}$. Indeed, due to this inaccuracy, we prefer not to use a sole linear model for the entire set $\mathcal{U}$ for the upcoming stability analysis. We will prefer another approach, which we will detail later on. Further details on the linearization results for both operating points can be found in Appendix A.1.
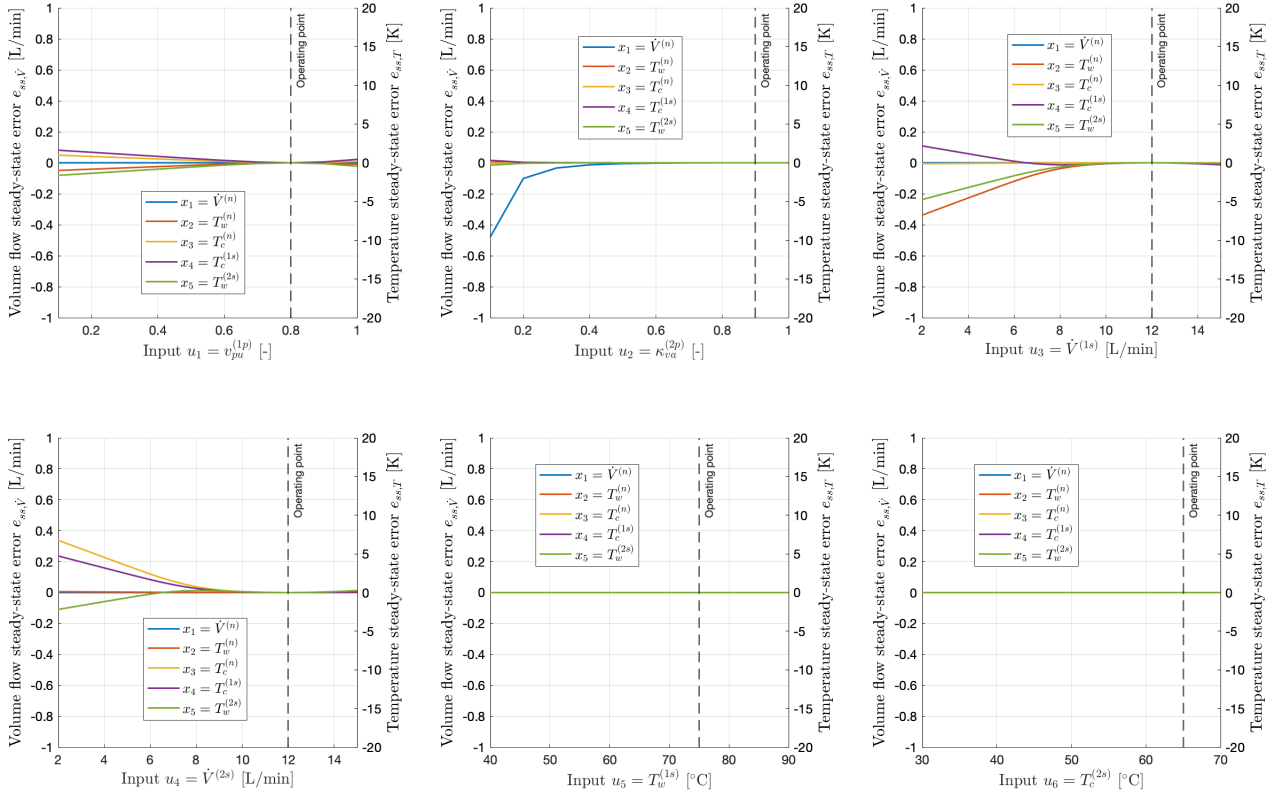
(a) Operating point 1
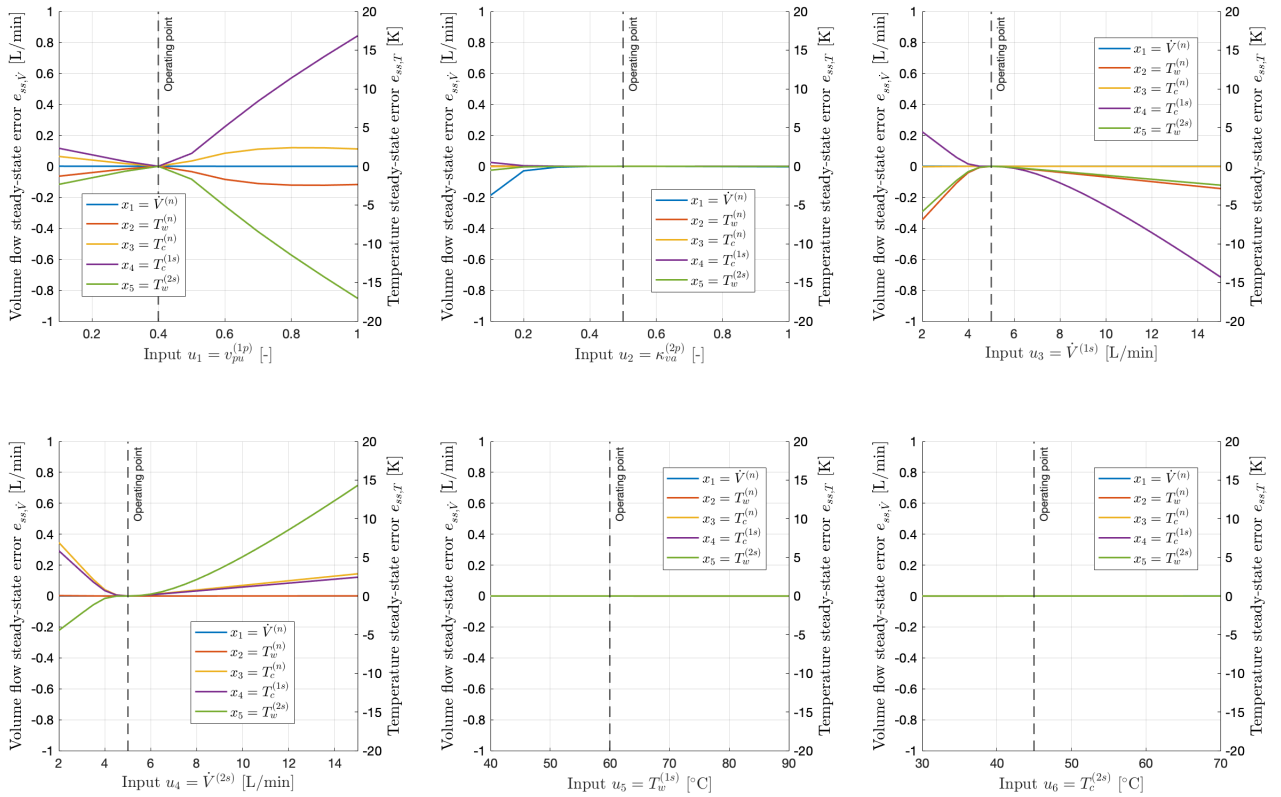
(b) Operating point 2

Figure 1.4: Absolute steady-state errors $e_{ss,\dot{V}}$ and $e_{ss,T}$ obtained by varying individual inputs. All other inputs are set to be at their operating point value.

Chapter 2

A PID-based control system for Smart Thermal Grids

As the Smart Thermal Grid should be operable in two directions, we need to make sure that the heat is indeed conveyed as desired. For this purpose, an Energy Management System determines the optimal energy exchange and checks the feasibility of the planned energy exchange. In case of a feasible solution, power setpoints are transmitted to the field controllers. The goal of these field controllers is then to meet both the temperature and heat transfer requirements simultaneously. For this pumps and valves in the system can be actuated.

In [6], a weighted PID-control approach has been developed to meet the combined control targets for both the primary and secondary side. In the following, this concept will be presented in more details.

2.1 Field control approach for the simplest case

The simplest case is constrained by some boundary conditions. Indeed, the temperatures coming into the buildings and flowing through the network must meet some physical value requirements in order to have a feasible system

$$T_w^{(1s)} > T_c^{(1s)} > T_w^{(n)} > T_c^{(n)} > T_w^{(2s)} > T_c^{(2s)} \tag{2.1}$$

Even though heat will shift from building 1 to building 2, the condition in (2.1) must also be met during the transfer process.

Setpoints We aim at regulating the warm water temperature at the consumer side. This temperature requirement is notated as $T_{w,set}^{(2s)}$. However, this setpoint alone does not constitute enough information for the Smart Thermal Grid to be able to reach it. Hence, setting a cold water temperature requirement on the producer side controls the heat that is fed into the network. This setpoint is set as the difference between the warm and cold temperatures at building 1: $\Delta T_{set}^{(1s)}$. Analogously, on the network side, we set the warm water temperature requirement as $T_{w,set}^{(n)}$ and the heat that is to be fed to the consumer as $\Delta T_{set}^{(n)}$. At the same time, we control the heat flow that is exchanged through the heat exchangers. As we assume no losses according to Assumption 2, we have only one setpoint notated as $\dot{Q}_{set}^{(n)}$. The resulting vector of setpoints $\underline{r}$ is thus

$$\underline{r} = \begin{bmatrix} r_1 \\ r_2 \\ r_3 \\ r_4 \\ r_5 \end{bmatrix} = \begin{bmatrix} \dot{Q}_{set}^{(n)} \\ T_{w,set}^{(2s)} \\ \Delta T_{set}^{(n)} \\ \Delta T_{set}^{(1s)} \\ T_{w,set}^{(n)} \end{bmatrix} \tag{2.2}$$

The attentive reader will notice that these correspond to the output variables chosen in section 1.3.1. Indeed, this set of setpoints explains the selected outputs, that had previously been chosen to match the given

setpoints.

Weighted errors   In general, we define the error vector $\underline{e}$ as being the difference between setpoints and outputs: $\underline{e} = \underline{r} - \underline{y}$. We further differentiate two types of errors: temperature errors e_T and heat flow errors $e_{\dot{Q}}$, which are computed as follows

$$e_T = \frac{(\Delta)T_{set} - (\Delta)T_{is}}{|\Delta T_{nom}|} \quad \text{and} \quad e_{\dot{Q}} = \frac{\dot{Q}_{set} - \dot{Q}_{is}}{\left|\dot{Q}_{nom}\right|} \tag{2.3}$$

Here we talk about normalized errors as they are further devided by their nominal value. For each set of temperature and heat flow setpoints, hence normalized error, the resulting weighted error function e_{tot} is computed as

$$e_{tot} = \pm\alpha e_{\dot{Q}} \pm (1 - \alpha)\, e_T \quad \text{with} \quad \alpha \in [0, 1] \tag{2.4}$$

We call α a weighting factor whose value can be chosen between 0 and 1 and serves to nuance the importance of the heat flow control with respect to the temperature control. As we have four different temperature requirements, we get four weighted error results, which are all obtained with respect to the sole heat flow requirement.

PID controllers   These weighted errors are further used as input to the PID controllers. Here, we choose to set their derivative term to zero, hence we get "only" PI controllers, which have the following generic transfer function

$$G_{PI}(s) = K_P + K_I \cdot \frac{1}{s} = \frac{K_P s + K_I}{s} \tag{2.5}$$

K_P and K_I represent the controller gains, that are used to tune the controller. In our case, we assume that those gains are equal for all four controllers.

The output values from the PID controllers represent the system inputs $\underline{u}$. Since, we expect bounded inputs into the Smart Thermal Grid (e.g. the normalized pump and valve control variables), we add a saturation to the PID-controllers, so that their output is always comprised between 0 and 1 – realistically to account for the feasibility of the simulation, we set the lower bound to 0.1 instead of 0. For the secondary side volume flow inputs, however, values can go from zero to a system dependent maximal value $\dot{V}_{max}$, which is the same in our case for both buildings. We then scale the normalized PID-controller output with this maximal value to obtain a valid volume flow input.

Block diagram   Finally, the completed block diagram for the previously presented control approach can be found in Figure 2.1. Inputs associated with the consumer/ producer side are separated by a dashed line. The block Smart Thermal Grid is represented by the nonlinear state-space representation established in section 1.3.1 or can be replaced by its linearized equivalent from section 1.3.2. The different values used as control parameters in our setup are given in Table 2.1.

Nominal values			
$\dot{V}_{max}$	8.5	L/m	nom. sec. side volume flow
$\dot{Q}_{nom}$	1	kW	nom. heat flow
ΔT_{nom}	3	K	nom. temperature diff.
PID controller			
K_P	1.5	-	proportional gain
K_I	1/35	1/s	integral gain

Table 2.1: Control setup parameters

2.2   Temperature and heat flow control

As mentioned before the weighting factor α serves to modulate the weight of the temperature error e_T as opposed to the heat flow error $e_{\dot{Q}}$ in the weighting error function e_{tot}. As a result of having four weighted
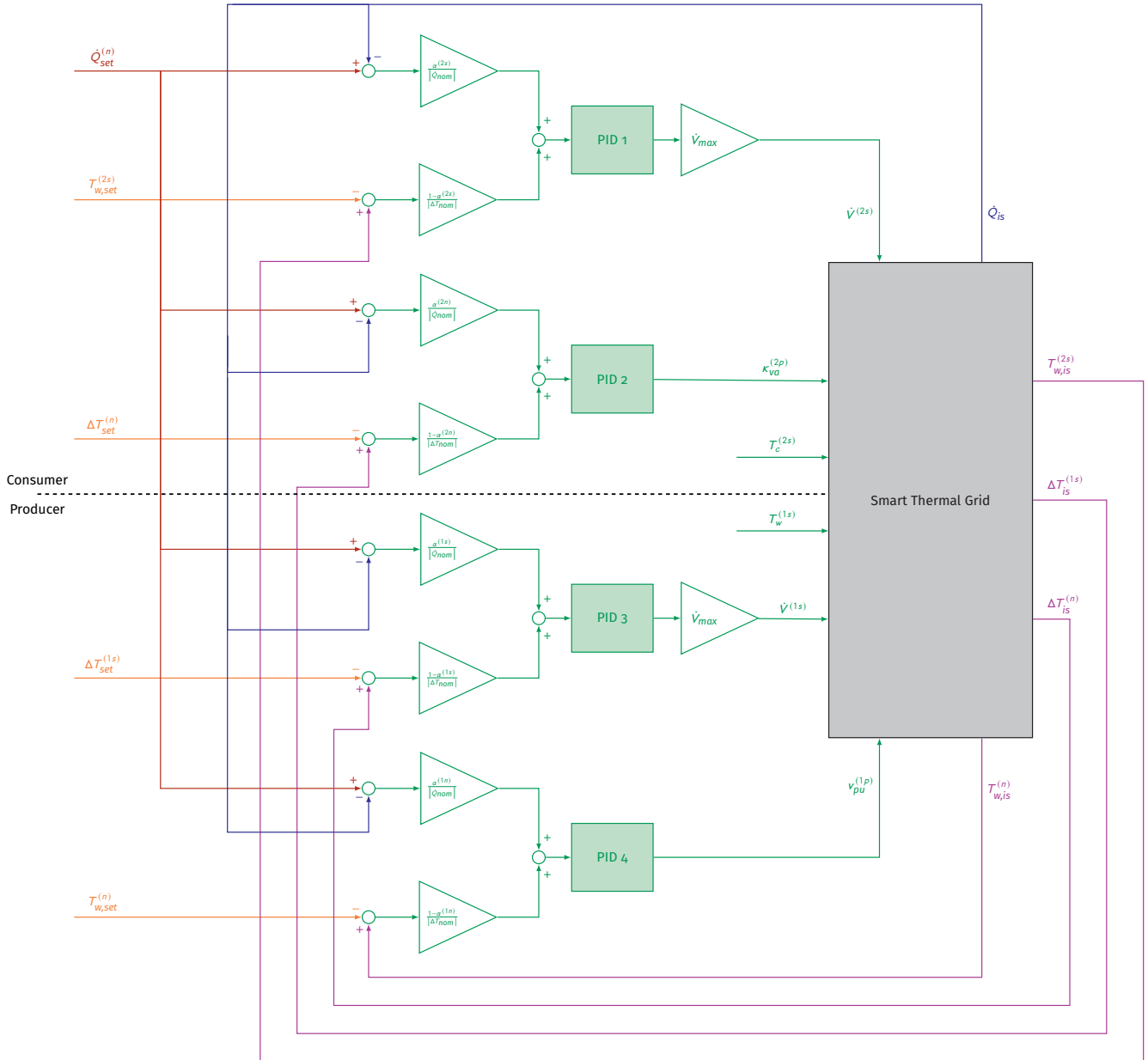
Figure 2.1: Weighted PID-based control approach for the simultaneous regulation of heat flow and temperatures

errors, we can choose four different values for α thus modifying the importance of buildings or network sides – secondary or primary side – in addition to the temperature/ heat flow compromise in the control process. It is possible to tune the following α parameters:

- $\alpha^{(1n)}$ – error weight for the primary side of building 1 i.e. the producer;

- $\alpha^{(1s)}$ – error weight for the secondary side of building 1 i.e. the producer;

- $\alpha^{(2n)}$ – error weight for the primary side of building 2 i.e. the consumer;

- $\alpha^{(2s)}$ – error weight for the secondary side of building 2 i.e. the consumer.

The exact role of these parameters in the control approach can be found in the block diagram in Figure 2.1.
    We can hence check the validity of our control approach by simulating different scenarios: 1) a temperature control only scenario, 2) a heat flow control only scenario and 3) a split control scenario. For the

following three scenarios, we set the setpoints to

$$\dot{Q}_{set}^{(n)} = 5\text{kW} \quad ; \quad T_{w,set}^{(2s)} = 40°\text{C} \quad ; \quad \Delta T_{set}^{(1s)} = 10\text{K} \quad ; \quad \Delta T_{set}^{(n)} = 14\text{K} \quad ; \quad T_{w,set}^{(n)} = 43.5°\text{C}$$

and the secondary side input volume flows to

$$u_5 = T_w^{(1s)} = 45°\text{C} \quad ; \quad u_6 = T_c^{(2s)} = 30°\text{C}$$

Temperature control only scenario   First, we simulate a temperature only control approach, since our ultimate goal is to regulate the warm water temperature on the consumer side. The weighting factors are thus set as

$$\alpha^{(1n)} = \alpha^{(1s)} = \alpha^{(2n)} = \alpha^{(2s)} = 0$$

This means that the weighting error function is solely constituted by the temperature errors. The system response of this scenario can be found in Figure 2.2a. It can be seen that except for the network warm water temperature none of the temperature objectives are reached. This is due to the fact that the system does not have enough information on the heat flow between the pipes, as is shown be the actual heat flow being far off from its target. Hence, heat flow control is also crucial for regulating the system temperatures.

Heat flow control only scenario   For this reason, we further try simulating a heat flow control only scenario with weighting factors

$$\alpha^{(1n)} = \alpha^{(1s)} = \alpha^{(2n)} = \alpha^{(2s)} = 1$$

The resulting weighting error function is only comprised of the heat flow error and Figure 2.2b shows the system response of the scenario. It becomes apparent that the heat flow objective is met quite precisely without any overshoot. However, the temperatures are far off from their respective setpoints. This is not surprising since in this scenario the PID-controllers have no information on the temperature errors and thus cannot regulate them. The importance of controlling both the temperatures and heat flows has been illustrated.
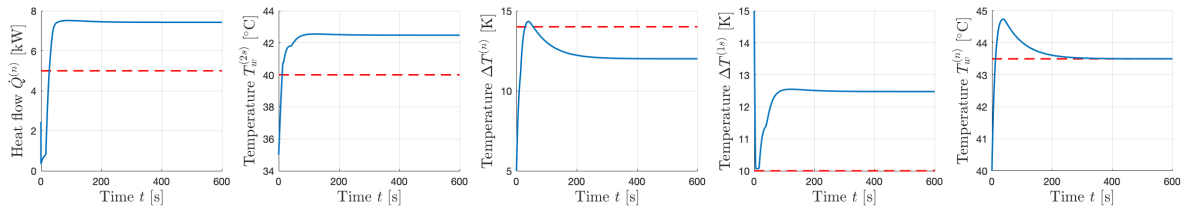
(a) Scenario 1 – Temperature control only
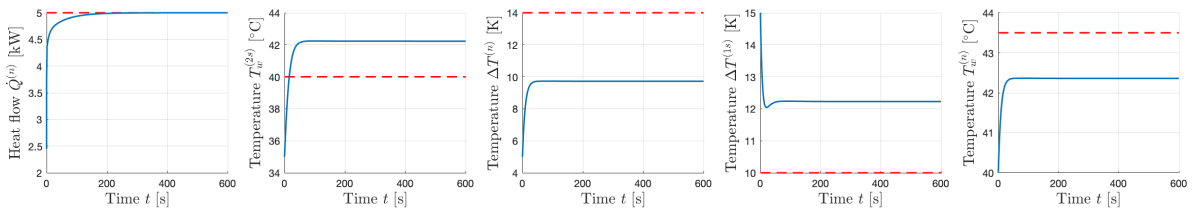
(b) Scenario 2 – Heat flow control only
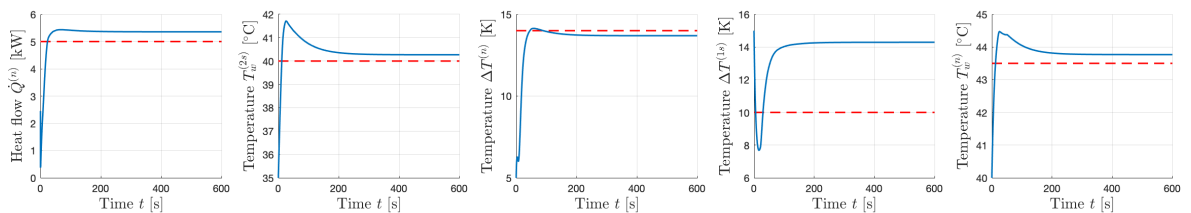
(c) Scenario 3 – Split control

Figure 2.2: System response (blue line) for each output of the nonlinear simulation model. The setpoint value is represented by a dashed red line.

Split control scenario Finally, we try controlling both heat flow and temperature at the same time by setting the weighting factors between 0 and 1

$$\alpha^{(1n)} = 0.2 \quad ; \quad \alpha^{(1s)} = 0.8 \quad ; \quad \alpha^{(2n)} = 0.8 \quad ; \quad \alpha^{(2s)} = 0.2$$

Here, we come up with a configuration that prioritizes absolute temperature objectives over temperature difference objectives. In parallel, the heat flow requirement becomes more important when having to meet a temperature difference setpoint, as it is more accurate to regulate the amount of heat that is transferred from one side of the heat exchanger to the other, as has been shown in the previous scenarios.

The resulting system responses are shown in Figure 2.2c. It can be seen that most requirements are met with only small deviations between desired and actual values. Especially the prioritized setpoints – the absolute temperature and heat flow requirements – are very close to their objectives. The still present errors are probably due to the "freedom" allowed by not considering the whole weight of the individual errors in the weighting error function e_{tot}. Concerning the less prioritized objectives, i.e. the temperature differences, we see that the temperature difference of the network is very close to the set requirement; thus it managed to mostly "regulate itself" by reaching the more important objectives as these are intricately linked. On the other hand, the temperature difference for the producer building 1 is far off from its objective. This is probably due to the fact that the setpoint is not reachable in combination with our other conditions. We also find that the temperatures overshoot before reaching steady-state, which is not very problematic as our system is not sensible in this aspect.

Chapter 3

Stability analysis of the control system

Running the Smart Thermal Grid with the field control approach we defined in the previous chapter, it is primordial to us to ensure a stable behavior of the system hence preventing e.g. oscillating temperatures. Goal of this chapter and more largely of the whole Research Internship is to find a method for proving (or not) stability of the grid. For this, we will first go through classical methods and their applicability to our case. We will then go on to statistical methods.

3.1 Formal stability criteria and applicability

Formal stability criteria are used for proving stability in any case taking into account some assumptions depending on the method. We will further investigate the relevance of some selected and more well-known methods to our study case.

3.1.1 Lyapunov's direct and indirect method

Very commonly used methods for proving stability are Lyapunov's stability methods, which comprise the direct and the indirect method.

Lyapunov's direct method   We will first give the theorem as has been enunciated in various literature articles – [7] and [8] being just some of them.

Theorem 1 (Lyapunov's direct method) *Consider an unexcited time-invariant nonlinear system $\underline{\dot{x}} = \underline{f}\left(\underline{x}, \underline{u} = \underline{0}\right)$ and $\underline{x}^* = \underline{0}$ an equilibrium point. Let $V(\underline{x})$ be a continuously differentiable and locally positive definite Lyapunov function.*

- *If $\dot{V}(\underline{x})$[1] ≤ 0 holds locally, then $\underline{x}^*$ is locally stable in the sense of Lyapunov.*

- *If $\dot{V}(\underline{x}) < 0$ holds locally, then $\underline{x}^*$ is locally asymptotically stable in the sense of Lyapunov.*

Should the assumptions above hold globally and should the system be radially unbounded, i.e. for $\|\underline{x}\| \to \infty$ it follows that $V(\underline{x}) \to \infty$, then $\underline{x}^*$ is globally (asymptotically) stable in the sense of Lyapunov.

The difficulty of this method resides in finding an appropriate Lyapunov function $V(\underline{x})$ which becomes increasingly more complex with the complexity of the considered system. Now, taking our own nonlinear state-space as formulated in (1.20), we quickly see that setting the input to zero to get the required unexcited system leads to a mathematical inconsistency. Indeed, for the first state we have

$$\dot{x}_1 = f_1\left(\underline{x}, \underline{u}\right) = -\frac{a_{hyd}}{\tau_{hyd}}x_1^2 - \frac{a_{2_{pu}}^{(1p)}}{\tau_{hyd}}u_1^2 - \frac{a_{va}^{(2p)}}{\tau_{hyd}}\frac{x_1^2}{u_2^2}$$

---

[1]$\dot{V}$ stands here for the derivative of the Lyapunov function and has nothing to do with the volume flow even though the notation is identical.

Yet it becomes quickly apparent that setting $u_2 = 0$ would lead to dividing by zero. Hence, we discard this method as inappropriate in our case, further keeping in mind that finding a suitable Lyapunov function would be close to impossible.

Lyapunov's indirect method   This method makes use of the linearization process of a nonlinear system to conclude on stability according to the eigenvalues of the system matrix $\underline{A}$. According to [8], the theorem can be formulated as follows.

Theorem 2 (Lyapunov's indirect method) *Again we take a time-invariant nonlinear system $\underline{\dot{x}} = \underline{f}\,(\underline{x}, \underline{u})$ with its equilibrium point $\underline{x}^* = \underline{0}$. We further require $\underline{f}(\underline{x}, \underline{u})$ to be twice continuously differentiable with respect to $\underline{x}$. Then the small signal behavior of the system around the equilibrium $\underline{x}^*$ can be written as follows (see section 1.3.2 for more details)*

$$\Delta \underline{\dot{x}} = \underline{A}\, \Delta \underline{x} \qquad with \qquad \underline{A} = \left[\frac{\partial \underline{f}\,(\underline{x}, \underline{u})}{\partial \underline{x}} \right]_{\underline{x} = \underline{x}^*} \tag{3.1}$$

The following conclusions can made on the equilibrium $\underline{x}^*$:

- *If all eigenvalues of $\underline{A}$ have a negative real part, then $\underline{x}^*$ is locally asymptotically stable in the sense of Lyapunov;*

- *If at least one eigenvalue of $\underline{A}$ has a positive real part, then $\underline{x}^*$ is locally unstable;*

- *If at least one eigenvalue of $\underline{A}$ has a null real part and no eigenvalue has a positive real part, then no conclusion can be drawn regarding the stability of $\underline{x}^*$.*

Having successfully managed to linearize the system in section 1.3.2, this method is in theory applicable to our problem. However, two major problems arise. The first one is that we saw that the linearization of the system generates high temperature errors for inputs far from the operating point. Hence, looking at the stability of the system via the indirect method of Lyapunov would only allow a local analysis around the operating point. The second more problematic issue lies in the fact that Lyapunov's stability analysis only takes into account the system in itself and not the control approach. Yet we would like to conclude on the control system in its whole as in Figure 2.1. For these two reasons we conclude that the method is not suitable for our needs.

3.1.2   Nyquist's stability criterion

Another widely used method is Nyquist's stability criterion. Now, as we consider a MIMO[2] system, we will directly present the generalized Nyquist criterion for MIMO systems (see [9, 10]), as it the one relevant to us. The more widely known criterion for SISO[3] systems can be found in [5].

Take a MIMO system described by a matrix of transfer functions $\underline{G}(s)$ as drawn in Figure 3.1. $\underline{L}(s)$ further defines the control transfer function matrix such that $\underline{u} = \underline{L}(s)\underline{e}$. Thus we can write

$$\underline{y} = \underline{G}(s)\underline{u} = \underbrace{\underline{G}(s)\underline{L}(s)}_{\underline{H}(s)}\,\underline{e} \tag{3.2}$$

with $\underline{H}(s)$ the loop matrix.

---

[2]Multiple Input Multiple Output.
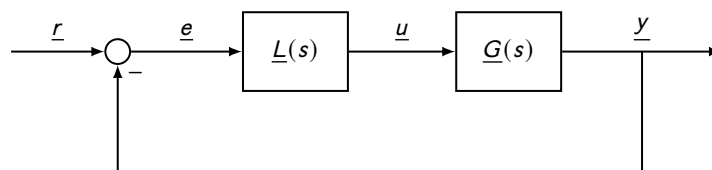[3]Single Input Single Output.

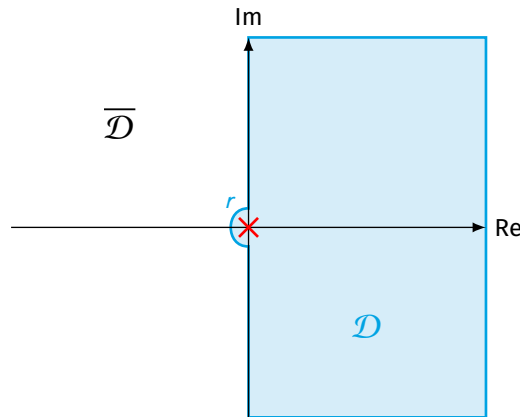Figure 3.1: Considered setting for the generalized Nyquist criterion

Figure 3.2: Definition of the contour $\mathcal{D}$ and its complement $\overline{\mathcal{D}}$
in case $\underline{H}(s)$ has one marginally unstable pole at the origin.

The MIMO Nyquist criterion, as we will present it in the following, has been formulated in [10] and uses Cauchy's principle of the argument [11]. Let it also be said before that a Nyquist diagram is represented for positive and negative frequencies by substitution of s by $j\omega$, with $-\infty < \omega < \infty$.

Theorem 3 (Generalized Nyquist criterion) *Consider the closed-loop unity negative gain feedback transfer function $\underline{S}(s) = \left(\underline{I} + \underline{H}(s)\right)^{-1}$. We further define $\mathcal{D}$ as the contour comprising possible unstable poles. It corresponds to the right-half plane including a small radius $r = \varepsilon$ with $\varepsilon \to 0$ indentation into the left-half plane around marginally stable poles of $\underline{H}(s)$ – i.e. around poles with a null real part – in order to include them as unstable poles. $\overline{\mathcal{D}}$ is the complement set to $\mathcal{D}$. Figure 3.2 illustrates this contour definition in the case that $\underline{H}(s)$ has one marginally unstable pole in the origin.*
The closed-loop system $\underline{S}(s)$ is exponentially stable if the following two conditions hold:

(i) $\det\left(\underline{I} + \underline{H}(s)\right) \neq 0, \quad \forall s \in \overline{\mathcal{D}}$;

(ii) the contour i.e. Nyquist diagram of $\det\left(\underline{I} + \underline{H}(s)\right)$ encircles the origin p_D times in a counter-clockwise direction, where p_D is the number of poles of $\underline{H}(s)$ in $\mathcal{D}$.

However, this method requires to have a linearized system. In our case, even though it is possible to convert the linearized state-space representation to a transfer function matrix $\underline{G}(s)$ and thus use the criterion accordingly, we will not be using this method directly as we do not consider our linearization to be representative of the whole system.

3.2 Monte Carlo based stability algorithms

We have seen that the most commonly used methods for assessing the stability of a system have proven to be unsuitable in our case in their "standard" form. This is especially due to the high nonlinearities in our system, which make a linearized version of it inaccurate over the whole considered interval of inputs. Yet, as we have seen in section 1.3.3 and A.1 and by definition, the linearization represents the system accurately in the operating point around which we linearize. Hence, by sampling the system over a high number of linearizations and assessing the stability for each linearization using the methods mentioned before, we should get a statistically accurate representation of the stability of the system and the input intervals on which it applies. The idea for this Monte-Carlo approach has been inspired by [12] and its basic functioning is presented in Algorithm 1.

We will now be applying (attempting to apply) this procedure using the stability criteria, we have discussed before and which apply to linear system i.e. Lyapunov's indirect method and Nyquist's stability criterion. We will further investigate using an extended state-space – the benefits of it shall be given in due course in section 3.2.3.

Algorithm 1:   Monte-Carlo stability approach

Data: $N > 0$;   /* N should have a high value e.g. 1000 or 10000 */
Result: vector of Booleans $\underline{b}_{stable}$;   /* indicates the stability for each iteration */
for $i = 1 \rightarrow N$ **do**
    sample $\underline{u}_{rand}$ uniformly in $\mathcal{U}$;
    simulate the nonlinear system with $\underline{u}_{rand}$ and get $\underline{x}_{ss}$;
    set the operating point to $\underline{x}^* = \underline{x}_{ss}$, $\underline{u}^* = \underline{u}_{rand}$;
    linearize the system around $\underline{x}^*, \underline{u}^*$;
    conduct a stability analysis on the linearized system ;   /* specified in the following */
    if *the linearization is stable* **then**
        $\underline{b}_{stable}(i) \leftarrow$ TRUE ;
    else
        $\underline{b}_{stable}(i) \leftarrow$ FALSE ;
    end
end
return $\underline{b}_{stable}$

3.2.1   Using Lyapunov's indirect method

As stated before, this method is solely useful for assessing the stability of the system in itself without including the control system as in Figure 2.1. So even though it does not suit our needs, it can give a first good indication on the stability, which is why we still mention it here.

We choose $N = 1000$ due to the limitations of the used hardware. Following the procedure of Algorithm 1, we get $\underline{b}_{stable}(i) =$ TRUE , $\forall i \in [1, N]$, which means that for all randomly sampled inputs $\underline{u} \in \mathcal{U}$ the Smart Thermal Grid is locally stable. We judge $N = 1000$ to be statistically meaningful enough to conclude that the system in itself as modelled in 1.2 is stable. This might not be true anymore if we do not consider all made simplifications e.g. if we account for losses or other delays in the model or if we consider more than just two prosumers.

3.2.2   Using the Nyquist criterion

As shown in [12], using Nyquist's stability criterion is manageable in this context. In order to be able to use the stability criterion as given in Theorem 3, we first need the control transfer function matrix $\underline{L}(s)$ so that the block diagrams in Figures 2.1 and 3.1 coincide. The error vector $\underline{e}$ stems from the difference between the reference and output vectors

$$\underline{e} = \underline{r} - \underline{y} = \begin{bmatrix} \dot{Q}_{set}^{(n)} - \dot{Q}_{is}^{(n)} \\ T_{w,set}^{(2s)} - T_{w,is}^{(2s)} \\ \Delta T_{set}^{(n)} - \Delta T_{is}^{(n)} \\ \Delta T_{set}^{(1s)} - \Delta T_{is}^{(1s)} \\ T_{w,set}^{(n)} - T_{w,is}^{(n)} \end{bmatrix} \tag{3.3}$$

The matrix $\underline{L}(s)$ is defined as given in section 3.1.2 such that $\underline{u} = \underline{L}(s)\underline{e}$. However, in our system, we have two inputs – u_5 and u_6 – which are in reality disturbances since we cannot control them. For now, we discard these two inputs and define a new input $\widehat{\underline{u}} = \begin{bmatrix} u_1 & u_2 & u_3 & u_4 \end{bmatrix}^T = \underline{L}(s)\underline{e}$. The expression of matrix $\underline{L}(s)$ stems directly from Figure 2.1

$$\underline{L}(s) = \underline{G}_{PI}(s) \, \underline{L}_{lin} = \underline{G}_{PI}(s) \begin{bmatrix} \frac{\alpha^{(1n)}}{|\dot{Q}_{nom}|} & 0 & 0 & 0 & -\frac{1-\alpha^{(1n)}}{|\Delta T_{nom}|} \\ \frac{\alpha^{(2n)}}{|\dot{Q}_{nom}|} & 0 & -\frac{1-\alpha^{(2n)}}{|\Delta T_{nom}|} & 0 & 0 \\ \dot{V}_{max} \frac{\alpha^{(1s)}}{|\dot{Q}_{nom}|} & 0 & 0 & -\dot{V}_{max} \frac{1-\alpha^{(1s)}}{|\Delta T_{nom}|} & 0 \\ \dot{V}_{max} \frac{\alpha^{(2s)}}{|\dot{Q}_{nom}|} & -\dot{V}_{max} \frac{1-\alpha^{(2s)}}{|\Delta T_{nom}|} & 0 & 0 & 0 \end{bmatrix} \tag{3.4}$$
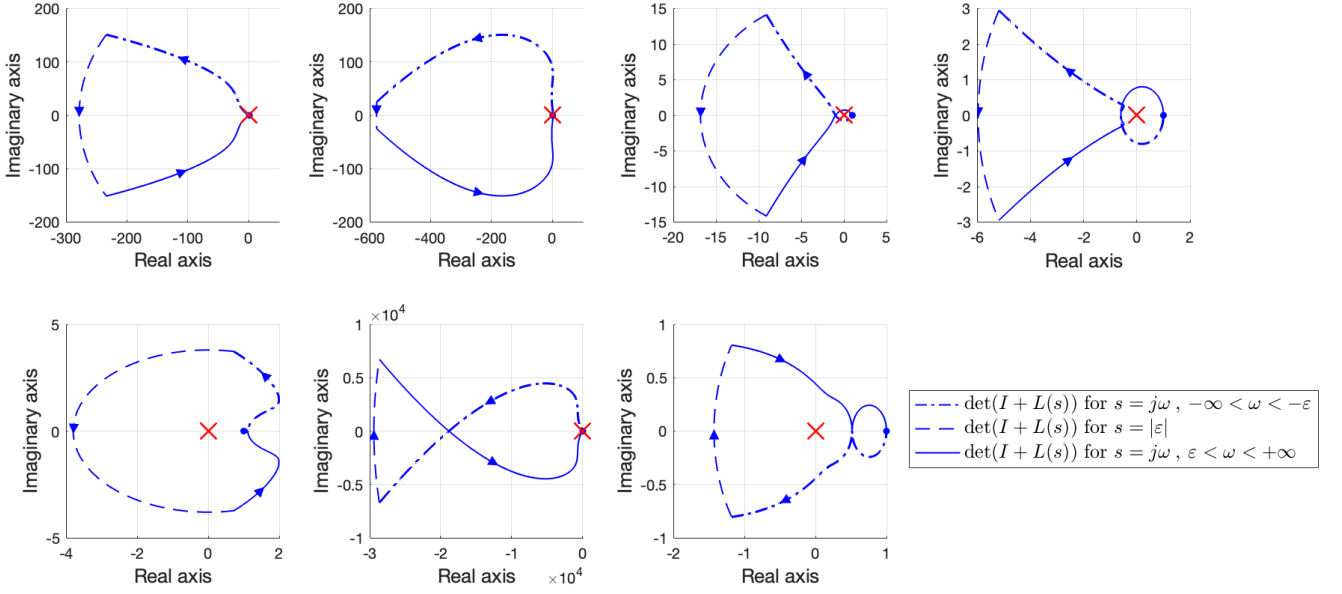
Figure 3.3: Nyquist diagram of det $(\underline{I} + \underline{H}(s))$ for $N = 7$ random input draws

The loop matrix $\underline{H}(s) = \widehat{\underline{G}}(s)\underline{L}(s)$ is then computed using the undisturbed system's transfer function matrix $\widehat{\underline{G}}(s)$ – the state-space $\{\underline{A}, \underline{B}, \underline{C}, \underline{D}\}$ is converted to a transfer function matrix $\underline{G}(s)$, where the columns associated with the disturbances are truncated to form a new matrix $\widehat{\underline{G}}(s)$, which does not consider the input-disturbances u_5 and u_6.

As defined in Theorem 3, we plot the Nyquist diagram of det $(\underline{I} + \underline{H}(s))$ in the hope of assessing its stability. Figure 3.3 shows this diagram for $N = 7$ iterations of Algorithm 1. The frequencies ω are split into three intervals drawn separately and the direction of the contour goes from $\omega \to -\infty$ to $\omega \to +\infty$ as indicated by the arrows. As defined in Theorem 3 and Figure 3.2, the ε arc goes to the left of any poles on the $j\omega$-axis. The critical origin point is indicated by a red cross. We can gather from the results in Figure 3.3 that the Nyquist diagram takes on a different shape depending on the random draw: it is thus particularly difficult to automate counting the number of couter-clockwise encirclements of the origin for a high number of Monte-Carlo algorithm iterations. Furthermore, we have 156 poles in our loop matrix $\underline{H}(s)$ from which 40 are marginally stable i.e. in $\mathcal{D}$. This magnitude of poles and the varying shapes make concluding solely "visually" on the Nyquist diagram an impossible task especially for the high number of iterations, which would be necessary to make statistically sound deductions.

In [13, 14], an equivalence between the Nyquist and Bode diagrams is proposed as a way to circumvent counting the number of couter-clockwise encirclements of the critical point, which gets increasingly complicated when the order of the system increases as in our case.

Theorem 4 (Generalized Bode criterion) *For this criterion, we require the loop matrix in* (3.2) *to be written in the following form* $\underline{H}(s) = \frac{N(s)}{D(s)}$ *with* $\underline{N}(s)$ *a transfer function matrix and* $D(s)$ *a polynomial. It is further required to be in Smith-McMillan form [14, 15], i.e. the denominator* $D(s)$ *should be a polynomial equal to the least common multiple of the denominators of all elements in* $\underline{H}(s)$. *The generalized Nyquist criterion then states that, provided there are no hidden unstable modes in the system, we can compute the number of closed-loop unstable poles* p_C, *i.e. the number of poles in the right-half plane, as*

$$p_C = p_O - n_A \tag{3.5}$$

with p_O *the number of unstable poles in the open-loop transfer matrix and* n_A *the total number of counter-clockwise encirclements around the critical point* $(-1, 0j)$ *of the Nyquist curves of all eigenvalues of* $\underline{H}(s)$.

Let us now trace an auxiliary ray in a random direction starting at $(-1, 0j)$. *The crossings between the Nyquist diagram and this ray can be used to rewrite the Nyquist criterion in* (3.5) *as*

$$p_C = p_O - \left(n_C^+ - n_C^-\right) \tag{3.6}$$

where n_C^+ represents the number of crossings between the Nyquist diagram and the ray when the phase is increasing and n_C^- when it is decreasing. The positive angle is defined in the counter-clockwise direction. Moreover, n_C^+ and n_C^- have to be calculated for each eigenvalue of $\underline{H}(s)$ and summed up in order to get the total number of encirclements.

As proposed in [13], tracing the ray starting from $(-1, 0j)$ on the real axis in direction of the negative values, allows for n_C^+ and n_C^- to be counted using the Bode diagram. They can hence be counted as crossings of the phase plot with $\pm(2k+1) \cdot 180°$, $k \in \mathbb{Z} - n_B^+$ indicating the crossings when the phase is increasing and n_B^- when it is decreasing. The Nyquist criterion (3.6) can be reformulated as

$$p_C = p_O - \left(2\left(n_B^+ - n_B^-\right) + n_B^0 \right) \tag{3.7}$$

The parameter n_B^0 accounts for eigenvalue crossings with $\pm(2k+1) \cdot 180°$ that may occur at $0\,\text{Hz}$ and cannot be counted in the Bode diagram. It can be taken from [14] how to determine this parameter.

Aiming at applying the generalized Bode criterion and already having an expression of the loop matrix $\underline{H}(s)$, the next step consists in converting $\underline{H}(s)$ to its Smith-McMillan form, which we attempt to do using the function `smform` of [15] in MATLAB. However, this creates an error which we did not manage to solve.

3.2.3 Using an extended state-space

We have seen that assessing the stability of the closed-loop system has proven difficult in our case especially due to the complexity of the system even using a linearization. We have further seen that employing system driven open-loop stability assessment methods – i.e. Lyapunov's indirect method – has proven much more convenient in our case. The purpose of using an extended state-space (see [16, 17]) then is to convert our closed-loop system to an equivalent open-loop one so as to use open-loop stability evaluation methods on it. This method also aims at circumventing the discarding of the disturbances as done before with the Nyquist criterion in section 3.2.2. This is crucial for the stability evaluation as the disturbances are part of the functioning of the Smart Thermal Grid.

For this, we need to separate our disturbance-inputs u_5 and u_6 from the rest of our inputs $\widehat{\underline{u}}$. The disturbances shall be denoted in the following as

$$\underline{d} = \begin{bmatrix} d_1 \\ d_2 \end{bmatrix} = \begin{bmatrix} u_5 \\ u_6 \end{bmatrix} \tag{3.8}$$

Hence, the linear state-space representation of (1.22), (1.23) can be rewritten as

$$\Delta\underline{\dot{x}} = \widehat{\underline{A}}\,\Delta\underline{x} + \widehat{\underline{B}}\,\Delta\widehat{\underline{u}} + \underline{E}\,\Delta\underline{d} \quad \Rightarrow \quad \underline{\dot{x}} = \widehat{\underline{A}}\left(\underline{x} - \underline{x}^*\right) + \widehat{\underline{B}}\left(\widehat{\underline{u}} - \widehat{\underline{u}}^*\right) + \underline{E}\left(\underline{d} - \underline{d}^*\right) \tag{3.9}$$

$$\Delta\underline{y} = \widehat{\underline{C}}\,\Delta\underline{x} + \widehat{\underline{D}}\,\Delta\widehat{\underline{u}} + \underline{F}\,\Delta\underline{d} \quad \Rightarrow \quad \underline{y} = \widehat{\underline{C}}\left(\underline{x} - \underline{x}^*\right) + \widehat{\underline{D}}\left(\widehat{\underline{u}} - \widehat{\underline{u}}^*\right) + \underline{F}\left(\underline{d} - \underline{d}^*\right) + \underline{y}^* \tag{3.10}$$

Due to our new "input distribution" as well as the new operating point $\underline{x}^*$, $\widehat{\underline{u}}^*$, $\underline{d}^*$ that arises from it, we get new expressions for the matrices in the representation

$$\widehat{\underline{A}} = \left.\frac{\partial f}{\partial \underline{x}}\right|_{\underline{x}^*, \widehat{\underline{u}}^*, \underline{d}^*} , \quad \widehat{\underline{B}} = \left.\frac{\partial f}{\partial \widehat{\underline{u}}}\right|_{\underline{x}^*, \widehat{\underline{u}}^*, \underline{d}^*} , \quad \underline{E} = \left.\frac{\partial f}{\partial \underline{d}}\right|_{\underline{x}^*, \widehat{\underline{u}}^*, \underline{d}^*} , \quad \widehat{\underline{C}} = \left.\frac{\partial h}{\partial \underline{x}}\right|_{\underline{x}^*, \widehat{\underline{u}}^*, \underline{d}^*} , \quad \widehat{\underline{D}} = \left.\frac{\partial h}{\partial \widehat{\underline{u}}}\right|_{\underline{x}^*, \widehat{\underline{u}}^*, \underline{d}^*} , \quad \underline{F} = \left.\frac{\partial h}{\partial \underline{d}}\right|_{\underline{x}^*, \widehat{\underline{u}}^*, \underline{d}^*}$$

We further denote the resulting extended state-space representation as

$$\underline{\dot{\widetilde{x}}} = \widetilde{\underline{A}}\,\widetilde{\underline{x}} + \widetilde{\underline{B}}\,\widetilde{\underline{u}} \tag{3.11}$$

$$\widetilde{\underline{y}} = \widetilde{\underline{C}}\,\widetilde{\underline{x}} + \widetilde{\underline{D}}\,\widetilde{\underline{u}} \tag{3.12}$$

Figure 3.4 illustrates via block diagrams the extended state-space approach: the closed-loop system is converted to an equivalent open-loop extended state-space. Now, we shall compute the equivalence leading to the extended state-space representation in (3.11) and (3.12). Two assumptions are to be made for this.

Assumption 3 (Extended state-space) *In order to be able to find an extended state-space, two assumptions[4] shall be made so as to facilitate the upcoming computational steps. First, we assume no change over time in the reference signal, i.e. $\underline{\dot{r}} = 0$, and, second, we assume this as well for the disturbances, i.e. $\underline{\dot{d}} = 0$.*

---

[4]These assumptions are not necessarily sensible with respect to the reality of the system, but shall still be made for now for simplification purposes.
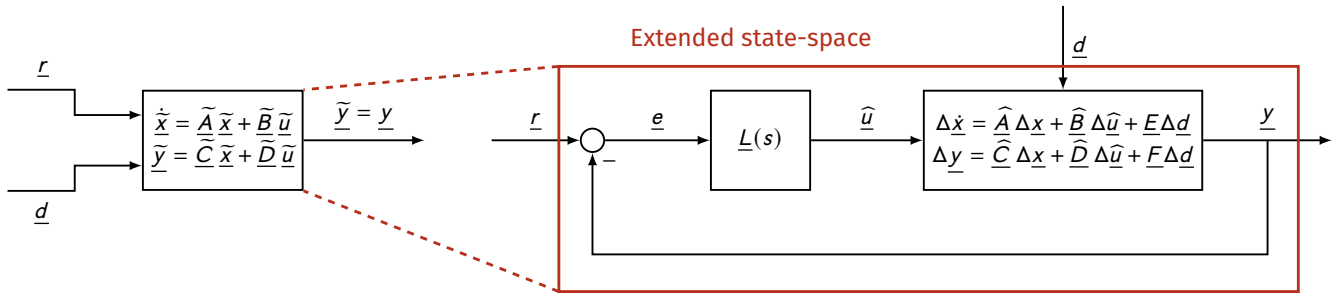
Figure 3.4: Block diagram of the extended state-space and its equivalence with the original closed-looped system

We know that $\widehat{\underline{u}} = \underline{L}(s)\,\underline{e}$ with $\underline{L}(s)$ as defined in (3.4). $\underline{L}(s)$ is the multiplication of the PI-transfer function $G_{PI}(s)$ in (2.5) with a matrix $\underline{L}_{lin}$, hence we can write

$$\widehat{\underline{u}} = \underline{L}(s)\,\underline{e} = G_{PI}(s)\,\underline{L}_{lin}\,\underline{e} = K_P\,\underline{L}_{lin}\,\underline{e} + K_I\,\underline{L}_{lin}\int \underline{e}\,\mathrm{d}t \tag{3.13}$$

From this, we can find an expression for the evolution of the error with respect to time, which translates the feedback loop of the system

$$\dot{\underline{e}} = \dot{\underline{r}} - \dot{\underline{y}} \tag{3.14}$$

Under Assumption 3, we have that $\dot{\underline{r}} = 0$, so this yields an expression for $\dot{\underline{e}}$

$$\dot{\underline{e}} = -\dot{\underline{y}} = -\widehat{\underline{C}}\,\dot{\underline{x}} - \widehat{\underline{D}}\,\dot{\underline{u}} - \underline{F}\underbrace{\dot{\underline{d}}}_{\substack{=0 \\ (\text{Ass. 3})}} = -\widehat{\underline{C}}\,\widehat{\underline{A}}\,(\underline{x} - \underline{x}^*) - \widehat{\underline{C}}\,\widehat{\underline{B}}\,(\widehat{\underline{u}} - \widehat{\underline{u}}^*) - \widehat{\underline{C}}\,\underline{E}\,(\underline{d} - \underline{d}^*) - \widehat{\underline{D}}\,\dot{\underline{u}}$$

$$= -\widehat{\underline{C}}\,\widehat{\underline{A}}\,(\underline{x} - \underline{x}^*) - \widehat{\underline{C}}\,\widehat{\underline{B}}\left(K_P\,\underline{L}_{lin}\,\underline{e} + K_I\,\underline{L}_{lin}\int \underline{e}\,\mathrm{d}t - \widehat{\underline{u}}^*\right) - \widehat{\underline{C}}\,\underline{E}\,(\underline{d} - \underline{d}^*) - \widehat{\underline{D}}\left(K_P\,\underline{L}_{lin}\,\dot{\underline{e}} + K_I\,\underline{L}_{lin}\,\underline{e}\right) \tag{3.15}$$

To get this expression we used the fact that the operating point does not change in time hence $\dot{\underline{x}}^* = \dot{\widehat{\underline{u}}}^* = \dot{\underline{d}}^* = \dot{\underline{y}}^* = 0$. Let us now introduce a new variable $\underline{e}' = \int \underline{e}\,\mathrm{d}t$. Equation (3.15) then becomes

$$\ddot{\underline{e}}' = -\widehat{\underline{C}}\,\widehat{\underline{A}}\,(\underline{x} - \underline{x}^*) - \widehat{\underline{C}}\,\widehat{\underline{B}}\left(K_P\,\underline{L}_{lin}\,\dot{\underline{e}}' + K_I\,\underline{L}_{lin}\,\underline{e}' - \widehat{\underline{u}}^*\right) - \widehat{\underline{C}}\,\underline{E}\,(\underline{d} - \underline{d}^*) - \widehat{\underline{D}}\left(K_P\,\underline{L}_{lin}\,\ddot{\underline{e}}' + K_I\,\underline{L}_{lin}\,\dot{\underline{e}}'\right)$$

$$\Leftrightarrow \quad \ddot{\underline{e}}' = -\left(1 + K_P\,\widehat{\underline{D}}\,\underline{L}_{lin}\right)^{-1}\left[\widehat{\underline{C}}\,\widehat{\underline{A}}\,(\underline{x} - \underline{x}^*) + \widehat{\underline{C}}\,\widehat{\underline{B}}\left(K_P\,\underline{L}_{lin}\,\dot{\underline{e}}' + K_I\,\underline{L}_{lin}\,\underline{e}' - \widehat{\underline{u}}^*\right) + \widehat{\underline{C}}\,\underline{E}\,(\underline{d} - \underline{d}^*) + K_I\,\widehat{\underline{D}}\,\underline{L}_{lin}\,\dot{\underline{e}}'\right] \tag{3.16}$$

Analogously to the error time derivative, it is possible to thus get an expression for the states and outputs of the system

$$\dot{\underline{x}} = \widehat{\underline{A}}\,(\underline{x} - \underline{x}^*) + \widehat{\underline{B}}\,(\widehat{\underline{u}} - \widehat{\underline{u}}^*) + \underline{E}\,(\underline{d} - \underline{d}^*) = \widehat{\underline{A}}\,(\underline{x} - \underline{x}^*) + \widehat{\underline{B}}\left(K_P\,\underline{L}_{lin}\,\dot{\underline{e}}' + K_I\,\underline{L}_{lin}\,\underline{e}' - \widehat{\underline{u}}^*\right) + \underline{E}\,(\underline{d} - \underline{d}^*) \tag{3.17}$$

$$\underline{y} = \widehat{\underline{C}}\,(\underline{x} - \underline{x}^*) + \widehat{\underline{D}}\,(\widehat{\underline{u}} - \widehat{\underline{u}}^*) + \underline{F}\,(\underline{d} - \underline{d}^*) + \underline{y}^* = \widehat{\underline{C}}\,(\underline{x} - \underline{x}^*) + \widehat{\underline{D}}\left(K_P\,\underline{L}_{lin}\,\dot{\underline{e}}' + K_I\,\underline{L}_{lin}\,\underline{e}' - \widehat{\underline{u}}^*\right) + \underline{F}\,(\underline{d} - \underline{d}^*) + \underline{y}^* \tag{3.18}$$

From these three equations – (3.16), (3.17) and (3.18) – we can get an extended state-space representation in the form (3.11), (3.12). We set our new state vector as $\widetilde{\underline{x}} = \begin{bmatrix}\underline{x} & \underline{e}' & \dot{\underline{e}}'\end{bmatrix}^T$ as well as our new input vector as $\widetilde{\underline{u}} = \begin{bmatrix}\underline{d} & \underline{x}^* & \widehat{\underline{u}}^* & \underline{d}^* & \underline{y}^*\end{bmatrix}^T$. Thus, we get the new state and input matrices

$$\widetilde{\underline{A}} = \begin{bmatrix} \widehat{\underline{A}} & K_I\,\widehat{\underline{B}} & K_P\,\widehat{\underline{B}} \\ 0 & 0 & 1 \\ -\left(1 + K_P\,\widehat{\underline{D}}\,\underline{L}_{lin}\right)^{-1}\widehat{\underline{C}}\,\widehat{\underline{A}} & -K_I\left(1 + K_P\,\widehat{\underline{D}}\,\underline{L}_{lin}\right)^{-1}\widehat{\underline{C}}\,\widehat{\underline{B}}\,\underline{L}_{lin} & -\left(1 + K_P\,\widehat{\underline{D}}\,\underline{L}_{lin}\right)^{-1}\left(K_P\,\widehat{\underline{C}}\,\widehat{\underline{B}} + K_I\,\widehat{\underline{D}}\right)\underline{L}_{lin} \end{bmatrix} \tag{3.19}$$

$$\widetilde{\underline{B}} = \begin{bmatrix} \underline{E} & -\widehat{\underline{A}} & -\widehat{\underline{B}} & -\underline{E} & 0 \\ 0 & 0 & 0 & 0 & 0 \\ -\left(1 + K_P\,\widehat{\underline{D}}\,\underline{L}_{lin}\right)^{-1}\widehat{\underline{C}}\,\underline{E} & \left(1 + K_P\,\widehat{\underline{D}}\,\underline{L}_{lin}\right)^{-1}\widehat{\underline{C}}\,\widehat{\underline{A}} & \left(1 + K_P\,\widehat{\underline{D}}\,\underline{L}_{lin}\right)^{-1}\widehat{\underline{C}}\,\widehat{\underline{B}} & \left(1 + K_P\,\widehat{\underline{D}}\,\underline{L}_{lin}\right)^{-1}\widehat{\underline{C}}\,\underline{E} & 0 \end{bmatrix} \tag{3.20}$$

along with our new output and feedthrough matrices

$$\widetilde{\underline{C}} = \begin{bmatrix} \widehat{\underline{C}} & K_I \, \widehat{\underline{D}} \, \underline{L}_{lin} & K_P \, \widehat{\underline{D}} \, \underline{L}_{lin} \end{bmatrix} \tag{3.21}$$

$$\widetilde{\underline{D}} = \begin{bmatrix} \underline{F} & -\widehat{\underline{C}} & -\widehat{\underline{D}} & -\underline{F} & 1 \end{bmatrix} \tag{3.22}$$

Having established the equivalence between the extended state-space and the closed-loop system, the next step consists in simulating both systems in order to find out if they really behave the same. Due to time constraints, this could not be part of the Research Internship anymore. We further attempted to compute the symbolic eigenvalues of the state matrix $\widetilde{\underline{A}}$ for applying Lyapunov's indirect method theoretically on the extended state-space representation. However, the computation proved to be too complex to do by hand or even on MATLAB even considering that in our case $\widehat{\underline{D}} = 0$ which allows for some simplifications.

3.3 Empirical considerations

Since during the time of the Research Internship we have not managed to conduct any satisfactory stability analysis, we want to make a few empirical considerations of the control system without following any formal method. We have seen in section 2.1, that we add a saturation to the PID-controller output such that its value stays in a range from 0 to 1 respectively $\dot{V}_{max}$. Considering this, it is thus impossible for our grid inputs and thus the whole system to diverge if the input-disturbances u_5 and u_6 stay in an acceptable range and follow condition (2.1). Indeed, theoretically, we could only observe for some cases a marginally stable behavior i.e. an oscillating behavior. Having thought of this control system property, a "proof" for having a marginally stable system could be to find one case where the system response oscillates. This would at least show that for our simplest case the Smart Thermal Grid is not entirely stable and would by extension not be for any more complex case.

Following this reasoning, we conduct a simple experiment which consists in simulating a high number of system responses of the control system in Figure 2.1 with uniformly randomly drawn setpoints, disturbances and weighting factors α, whereas condition (2.1) is ensured to be met. We then evaluate a possible marginally stable behavior visually. In our case, we impose the following conditions on the random draws

$$\dot{Q}_{set}^{(n)} \in [140, 63000]\text{W} \quad , \quad T_{w,set} \in [40, 90]°\text{C} \quad , \quad T_{c,set} \in [30, 70]°\text{C} \quad , \quad \alpha \in [0, 1] \qquad \text{s.t. (2.1) holds}$$

Figure 3.5 shows the output responses for 100 draws of this experiment. Even though the curves for each output vary considerably especially due to the different setpoints, none of them seem to show any abnormal behavior i.e. the output reaches steady-state without diverging or oscillating in any way. While this is by far not a proof of stability, we cannot prove any instability with this either. Appendix A.2 shows some further results of this experiment. It shall also be mentioned that when not ensuring condition (2.1), MATLAB stops the simulation due to the system being unstable and diverging. We can conclude from this that the feasibility condition (2.1) is thus a crucial condition for stability.

We further simulated the system response with steps/ ramps for the disturbances and steps for the setpoints instead of them remaining constant, but again this did not lead visually to any instability.
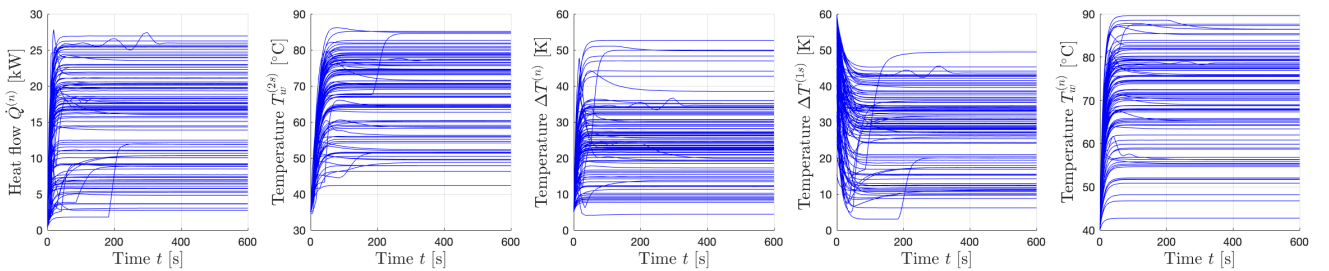

Figure 3.5: Output response for the closed-looped system in Figure 2.1 with 100 uniformly random draws of setpoints, disturbances and weighting factors. Setpoints and disturbances are constant.

Conclusion

In this report and more exactly during this Research Internship, we inspected a bi-directional heat transfer system linking different prosumers in an urban area. This setup enables a more optimal way of controlling a heating grid and is part of the process of local decarbonization through Smart Grids. Throughout the report, we only considered the simplest case of two prosumers, one acting as a producer and the other as a consumer. Hopes of extending our findings to more than two prosumers could not be met due to time constraints but could, however, be investigated in further work.

Our contribution to the analysis of Smart Thermal Grids was to assess (attempting to assess) the stability of the control of such a system. In order to do so, we proceeded in three steps which were modeling the simplest case of a bi-directional heat transfer system, setting up the field control approach and applying stability analysis methods on the system.

Modeling the simplest case   In a first step, we sought to model the Smart Thermal Grid in case of two prosumers. For this, we established the equations for the hydraulic and the thermal subsystems separately – both subsystems are linked through the heat exchangers. We considered the grid's components individually and applied Kirchhoff's mesh and junction rules to obtain an overall representation with five dynamic equations describing the whole thermohydraulic heat transfer system. It shall also be mentioned that we did not account for any losses in the system and considered a delay in the volume flow through pumps and valves only for simplification purposes. However, these simplifications do not reflect reality and should be taken into account for more a more meaningful analysis.

We then converted the dynamic equations to a nonlinear state-space representation after having defined our states, inputs and outputs. As for many stability evaluation methods, one needs a linear system, we aimed at linearizing the nonlinear system around an operating point. However, a linearization only represents a planar approximation around the operating point and can differ considerably from the nonlinear system when straying away from this operating point. For this reason, we evaluated the steady-state errors in our states following the linearization for the whole considered set of acceptable inputs. We compared two operating points – one with high volume flows and temperatures and one with lows volume flows and temperatures – and found that for either linearization the resulting errors were too important to consider the linearization as valid on the entire input interval. Only very close to the operating point did the linear system response coincide with the nonlinear one.

Field control approach   Controlling the Smart Thermal Grid is crucial for a successful heat transfer since the network can be operated in two directions. For this a weighted PID-control approach has been developed for meeting both the temperature and heat flow requirements of both building sides. The weighted normalized errors of temperatures and heat flow – instead of the "usual" feedback errors – were used as an input to PID-controllers with a null derivative term. The PID-controller outputs then functioned as the system's inputs and were further bounded so as to comply with the physical limitations of the system. A simulation of the control system showed the role of the weighting factors for meeting the requirements.

Stability analysis   The core of the Research Internship resided in assessing the stability of the field control approach. Such an evaluation is important to ensure the reliable and accurate behavior of the Smart Thermal Grid. For this, two criteria were important to us: 1) evaluating the stability of the whole control system not only the Smart Thermal Grid and 2) evaluating the stability for the entire set of possible inputs. Different methods have been investigated without leading to satisfying results, however, they could lay the foundation for future work on the subject.

The only contemplated approach that can be directly applied to nonlinear systems has been Lyapunov's direct method, which, however, solely enables to asses the stability for the unexcited thermohydraulic system. Moreover, it requires finding a suitable Lyapunov function, which in light of the complexity of the Smart Thermal Grid system we contemplated – even if we only considered the simplest case – proved to be almost impossible. Furthermore, for this method, we needed to work with the unexcited system which further lead to a mathematical incoherence rendering the use of Lyapunov's direct method impossible in our case.

Other formal methods like Lypunanov's indirect method and Nyquist's stability criterion can only be applied on linear systems, yet we have deemed our linearization not to be meaningful enough on the entire set of possible inputs to apply these criteria. Moreover, with Lyapunov's indirect method as for Lypunov's direct method only the stability of the thermohydraulic system in itself can be investigated.

Due to the lack of accuracy of the linearized system over the whole considered interval of inputs, we next thought about a Monte-Carlo approach, where we randomly sampled a great number of operating points and linearized the system around them. As we have seen that around the operating point, linear and nonlinear system behavior coincides, evaluating the stability of a lot of linearizations on the allowed set of inputs gives a statistically good indication on the stability of the whole nonlinear system. In this sense, we have devised an algorithm for applying this approach – the only problem that remained to be solved was which method to apply for analyzing the stability of one linearization. A first method, we applied was Lyapunov's indirect method. We found that for all sampled linearizations the thermohydraulic system in itself proved to be stable. Even though this was a first good indication on the stability of the whole system it did not fit with our criteria, hence we sought to apply other methods better suited to our needs.

As Nyquist's stability criterion fitted all our requirements, we tried to apply it to our system. The latter having multiple inputs and multiple outputs, however, we needed to use the generalized Nyquist criterion. Even though we succeeded in plotting the Nyquist diagram for the system, it proved to be too complicated and different for each sample to automate the process of counting the number of counter-clockwise encirclements of the origin. Hence, we looked for another way to apply the criterion, which we found in the generalized Bode criterion. Indeed, by drawing up an equivalence between Nyquist and Bode diagram, it is possible to find a more systematic way of counting the number of unstable poles of the system. However, this method required to find the Smith-McMillan form of our transfer function matrix. We did not succeed in this as we suspect that the system we considered was too complex. Another problem with Nyquist's stability criterion resided in including disturbances in our analysis, as indeed two of our six defined inputs could be more accurately referred to as disturbances since they were not directly controlled by our weighted PID-controller approach.

Our final idea was to convert our closed-loop system to an equivalent open-loop one, in order to apply open-loop stability methods like Lyapunov's indirect method on the equivalent open-loop system. We called this equivalent open-loop system extended state-space. We were successful in computing the equivalence between both representations, however, due to time constraints, we could not simulate them to find out if indeed they showed equivalent system responses. Attempts to apply Lyapunov's indirect method theoretically were not fruitful as the computations were too complicated to do symbolically. Moreover, some simplifications were again made in order to find the equivalence between both representations, which do not necessarily reflect reality.

In the end, we resorted to conduct a few empirical considerations. So we summarized that due to the bounded PID-controller outputs, the system could not diverge but only be marginally stable i.e. oscillating. Yet, we could not experimentally find a case where the system showed such a behavior when the feasibility of control requirements was guaranteed. This however is by no means a proof of stability.

Future work   Considering all our findings, we want to make a list of possible approaches and starting points for future work on the subject:

1. Find a way to convert the loop transfer function matrix to its Smith-McMillan form in order to be able to apply the generalized Bode criterion. If such can be done, deal with including the disturbance-inputs of the system in the analysis.

2. Confirm by simulation the equivalence between the extended state-space and the original closed-loop system. If an equivalence can indeed be shown, Lyapunov's indirect method might be suitable to account for the stability of the system in the context of the devised Monte-Carlo approach. If this

is successful, a new equivalence could be found without the assumptions made on the system for simplification.

3. Investigate new possible stability assessment methods such as a passivity analysis or splitting the system into interconnected subsystems.

4. Should it be possible to assess the stability for the simplest case, it could be expanded to cover more prosumers – proving the stability additionally for three prosumers in line and in a triangle should be enough to account for every possible formation of two or more prosumers. Moreover, losses and further delays could be added to the model of the grid.

In any case succeeding in assessing the stability of the field control approach for Smart Thermal Grids is a necessary step for paving the way for Smart Grids in general. Indeed, if we want to implement such grids in reality, we have to make sure of their reliable operation, which also passes through the stability of the system and its control. As it is, we also need to make sure that we conduct our stability analysis on a model as close to reality as possible so as to make it a conceivable and mature solution for the future.

Bibliography

[1] Vedran S Perić, Thomas Hamacher, Anurag Mohapatra, Franz Christiange, Daniel Zinsmeister, Peter Tzscheutschler, Ulrich Wagner, Christian Aigner, and Rolf Witzmann. Coses laboratory for combined energy systems at tu munich. In *2020 IEEE Power & Energy Society General Meeting (PESGM)*, pages 1–5. IEEE, 2020.

[2] Thomas Licklederer, Thomas Hamacher, Michael Kramer, and Vedran S Perić. Thermohydraulic model of smart thermal grids with bidirectional power flow between prosumers. *Energy*, 230:120825, 2021.

[3] Tracy Dalton, Ron J Patton, and JH Paul Millar. Methods of fault detection for a centrifugal pump system. *IFAC Proceedings Volumes*, 28(12):123–128, 1995.

[4] Piotr Laszczyk. Simplified modeling of liquid-liquid heat exchangers for use in control systems. *Applied Thermal Engineering*, 119:140–155, 2017.

[5] Martin Buss. *Regelungssysteme 1*. Lehrstuhl für Steuerungs- und Regelungstechnik, Technische Universität München, 2019.

[6] Thomas Licklederer, Daniel Zinsmeister, and Vedran Peric. A field-level control approach for bidirectional heat transfer stations in prosumer-based thermal networks. In *Presentation at 8th Internation Conference on Smart Energy Systems*, 2022.

[7] Hassan K Khalil. Lyapunov stability. *Control systems, robotics and automation*, 12:115, 2009.

[8] Martin Buss. *Dynamische Systeme*. Lehrstuhl für Steuerungs- und Regelungstechnik, Technische Universität München, 2021.

[9] C Desoer and Yung-Terng Wang. On the generalized Nyquist stability criterion. *IEEE Transactions on Automatic Control*, 25(2):187–196, 1980.

[10] Roy Smith. *A MIMO Nyquist Stability Test Example*. ETH Zürich, 2015.

[11] John M Howie. Cauchy's Theorem. *Complex Analysis*, pages 107–117, 2003.

[12] Yaran Wang, Shijun You, Huan Zhang, Xuejing Zheng, Shen Wei, Qingwei Miao, and Wandong Zheng. Operation stability analysis of district heating substation from the control perspective. *Energy and Buildings*, 154:373–390, 2017.

[13] M Vidyasagar, RK Bertschmann, and CS Sallaberger. Some simplifications of the graphical nyquist criterion. *IEEE transactions on automatic control*, 33(3):301–305, 1988.

[14] Javier Samanes, Andoni Urtasun, Ernesto L Barrios, David Lumbreras, Jesús López, Eugenio Gubia, and Pablo Sanchis. Control design and stability analysis of power converters: The MIMO generalized bode criterion. *IEEE Journal of Emerging and Selected Topics in Power Electronics*, 8(2):1880–1893, 2019.

[15] Oskar Vivero. MIMO Toolbox For Use with MATLAB, 2006.

[16] Ridong Zhang, Anke Xue, and Furong Gao. *Model predictive control: Approaches based on the extended state space model and extended non-minimal state space model*. Springer, 2018.

[17] Anurag Mohapatra, Vedran S Perić, and Thomas Hamacher. Formal verification of grid frequency controllers. In *2021 IEEE PES Innovative Smart Grid Technologies Europe (ISGT Europe)*, pages 01–06. IEEE, 2021.

Appendix

A.1 Further details on the linearization analysis

This appendix aims at providing more details on the linearization evaluation discussed in section 1.3.3. We consider the same two operating points as defined in Table 1.3 of before mentioned section.

This further analysis is based on a visual evaluation of the system behavior of the nonlinear and linear state-space representations for both operating points. Figure A.1 shows the time response for each state and model and figure A.2 their output behavior. The state and output dynamics are seemingly identical for both operating points and both representations. This is to be expected since the input vector $\underline{u}$ used for simulation is the same as used for linearizing the system. Indeed, in this case, we are located at the intersection between planar approximation and nonlinear multidimensional system dynamics surface. This visual evaluation shows us that our linearization is valid around the operating point.

This fact is of further interest to us for the stability analysis in chapter 3, as we can model our nonlinear system by a linear system around a given operating point and thus facilitate the stability analysis for this operating point. Doing this for a large set of operating points, we can have a statistical conclusion concerning the stability of our (controlled) system.

A.2 Further details on the empirical considerations

This appendix is a complement to the empirical considerations in section 3.3 and shows the results for some more precise experiments.

Random disturbances   First, we consider an experiment with random disturbances drawn from a uniform distribution, yet, we still ensure that condition (2.1) is met. The setpoints are identical and constant, having the same value as defined in section 2.2, for each draw. The weighting factor values are set to $\alpha^{(1n)} = 0.2$, $\alpha^{(1s)} = 0.8$, $\alpha^{(2n)} = 0.8$, $\alpha^{(2s)} = 0.2$. Figure A.3a shows the results of the experiment for 100 random disturbance draws. It can be seen that even though depending on the disturbances the target values are more or less met, the system behavior is stable and always shows a similar response shape. It is interesting to notice that since we chose setpoints at low temperature levels, the steady-state is often reached at higher temperatures but never below the setpoints. We conclude from this that it seems like the disturbances do not influence the stability of the system but only the quality of the control when they are set such that the feasibility of the system is guaranteed.

Random weighting factors   As a second experiment, we want to see if random weighting factors α can "destabilize" the system. Hence, we set the factors randomly in their allowed interval $[0, 1]$. The disturbances are set as defined in section 2.2 as are the setpoints. Figure A.3b shows the results for 100 draws. Again we do not distinguish any unstable system behavior even though the target values are seldom met. This could be expected since the weighting factors only play a role in the computation of the error inputs for the PID-controllers by giving either the temperature error or the heat flow error more weight. Hence, they can only play a role in the control quality but cannot render the system to be unstable.

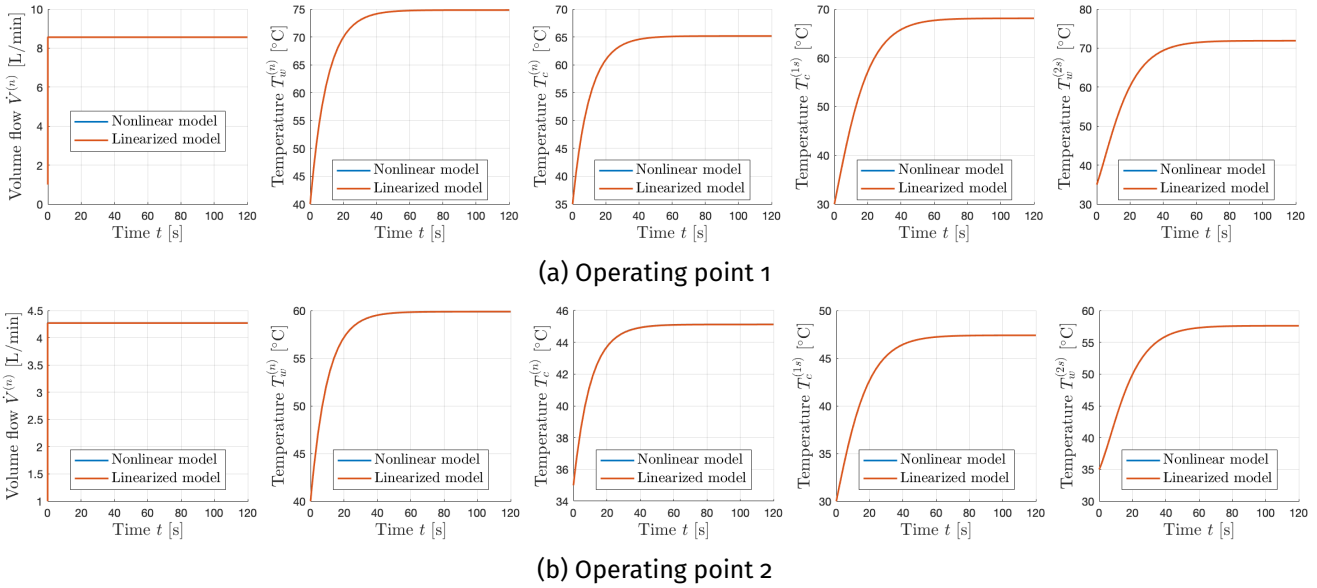(a) Operating point 1

(b) Operating point 2

Figure A.1: System response for each state of the nonlinear and linearized model. The system is actuated by constant inputs fixed at the operating point value.
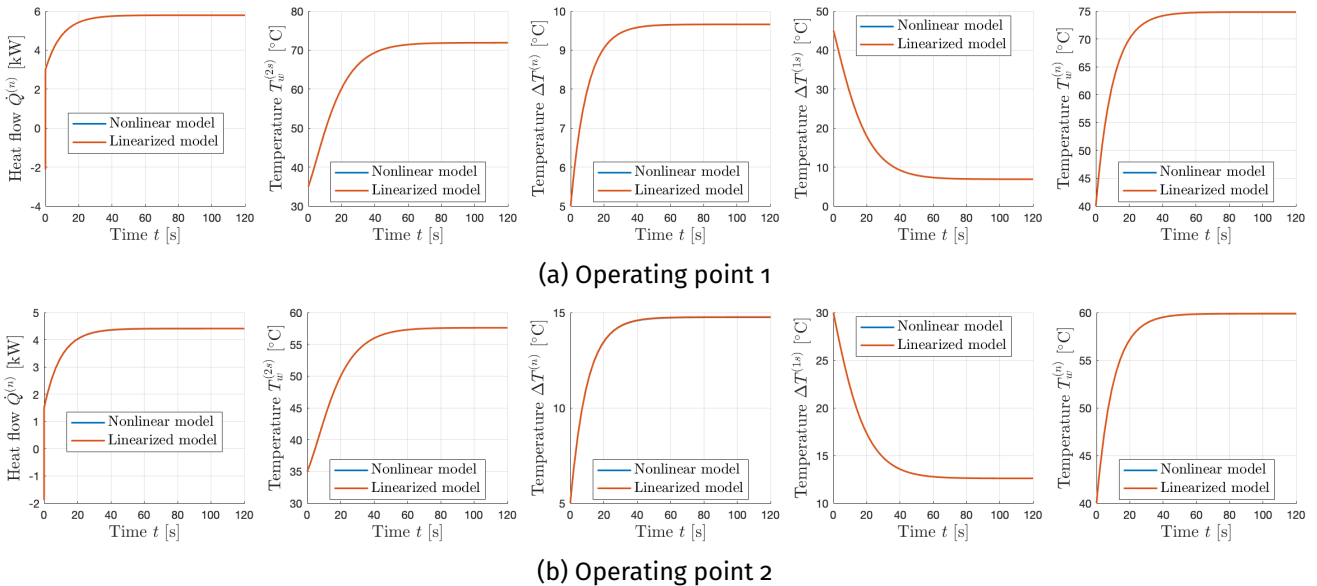

(a) Operating point 1

(b) Operating point 2

Figure A.2: System response for each output of the nonlinear and linearized model. The system is actuated by constant inputs fixed at the operating point value.
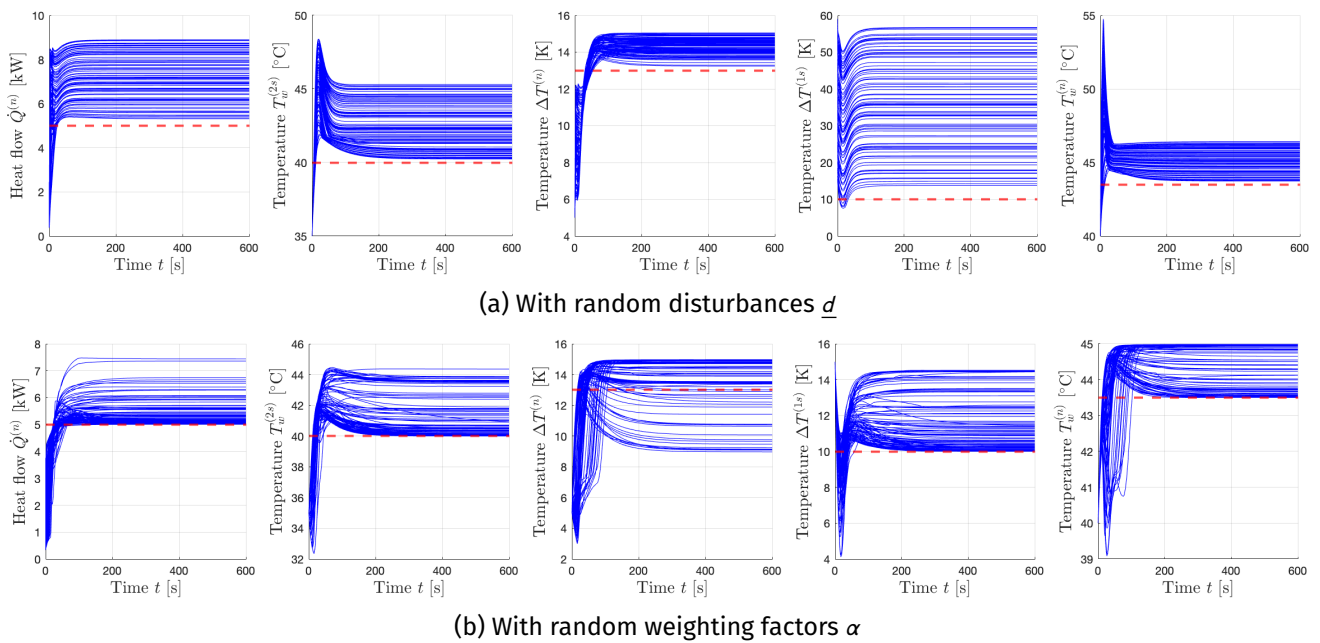
(a) With random disturbances $\underline{d}$

(b) With random weighting factors α

Figure A.3: Output response of the closed-looped system of Figure 2.1 when choosing one randomly drawn parameter from a uniform distribution. 100 draws (blue lines) were made for these plots. The setpoints stay the same in both experiments and are indicated by a red dashed line.